

A double-resolution transient RCM climate change simulation experiment for near-coastal eastern zone of the Eastern Mediterranean region

S. O. Krichak · J. S. Breitgand · R. Samuels · P. Alpert

Received: 25 September 2008 / Accepted: 3 March 2010 / Published online: 18 May 2010
© Springer-Verlag 2010

Abstract A double-resolution regional experiment on hydrodynamic simulation of climate over the eastern Mediterranean (EM) region was performed using an International Center for Theoretical Physics, Trieste RegCM3 model. The RegCM3 was driven from the lateral boundaries by the data from the ECHAM5/MPI-OM global climate simulation performed at the MPI-M, Hamburg and based on the A1B IPCC scenario of greenhouse gases emission. Two simulation runs for the time period 1960–2060, employing spatial resolutions of 50 km/14 L and 25 km/18 L, are realized. Time variations of the differences in the space distributions of simulated climate parameters are analyzed to evaluate the role of smaller scale effects. Both least-square linear and non-linear trends of several characteristics of the EM climate are evaluated in the study. One of the key findings with regard to linear trends is a notable and statistically significant precipitation drop over the near coastal EM zone during December–February and September–November. Statistically significant positive air temperature trends are projected over the entire EM region during the four seasons. Also projected are increases in air temperature extremes and the relative contribution of convective processes in the Southern Mediterranean coastal zone (ECM) region. A notable sensitivity of projected larger-scale climate change signals to smaller-scale effects is also demonstrated.

1 Introduction

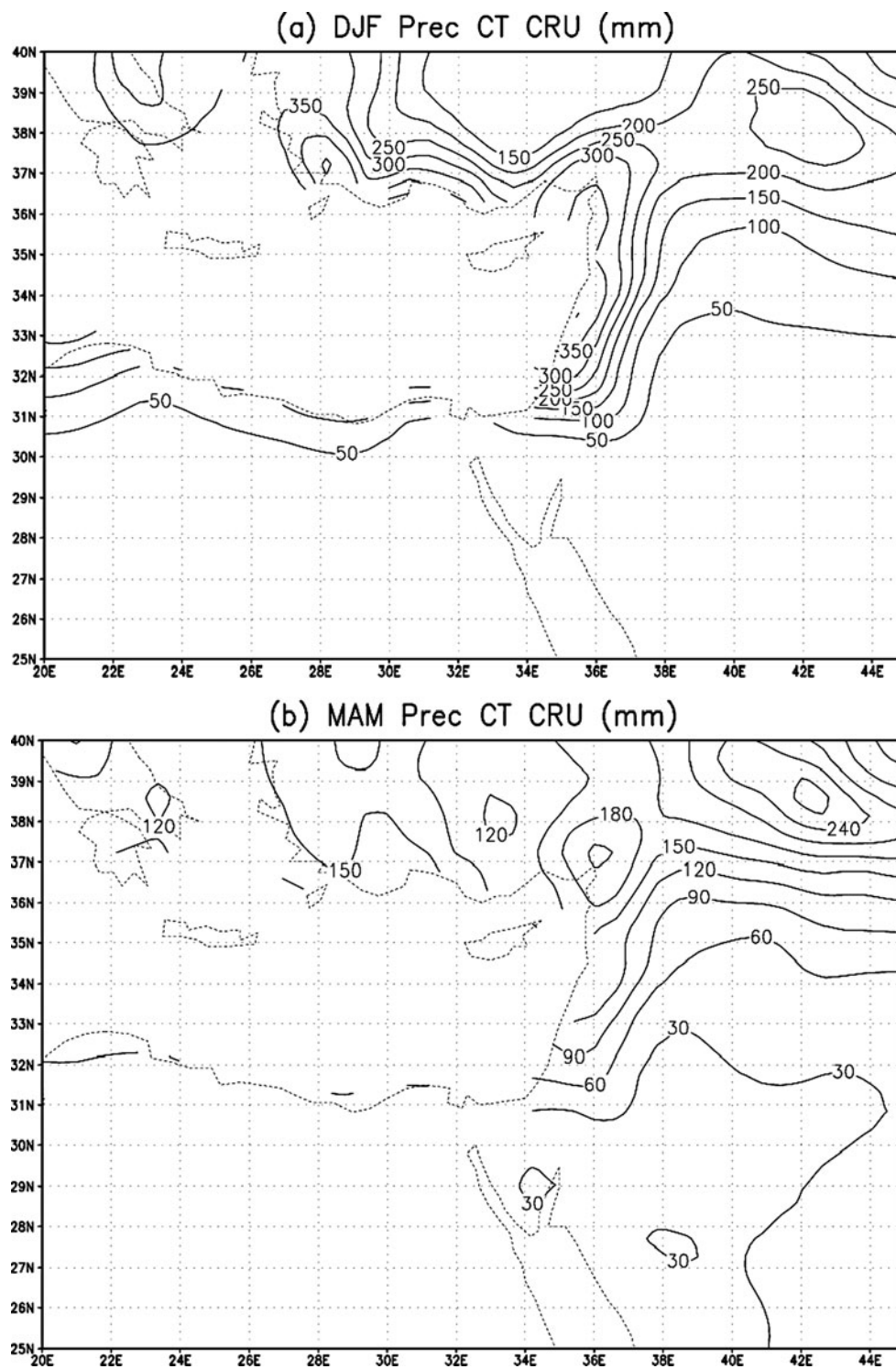
Evaluations of climate change trends due to effects of anthropogenic emission of greenhouse gasses (GHG) are

usually performed with the help of Atmosphere-Ocean Global Climate Models (AOGCM) using specially designed projections of future GHG emissions (IPCC 2001, 2007). Most of the contemporary AOGCMs are characterized by relatively coarse (~200 km or more) spatial resolution, precluding them from accounting for the contributions of small-scale atmospheric and land surface effects. Regional climate model (RCM) downscaling of the AOGCM results is often performed (e.g., Caya and Biner 2004; Christensen and Christensen 2003; Giorgi et al. 2004a, b; Gubasch, 2001; Jones et al. 1995, 1997; Takle et al. 2007; Pal et al. 2007; Wang et al. 2004) to deeper understand the AOGCM results over specific areas.

Notable peculiarities of climate conditions characterized by moderate air temperatures and changeable rainy weather during the cooler winter season and dry and stable hot weather during summer over the eastern Mediterranean region (EM) complicate the use of the RCM approach here (Evans et al., 2004; Pal et al., 2007; Krichak et al., 2007; Pal et al. 2007). To illustrate the characteristic of the EM climate, multiyear mean seasonal [December–February (DJF), March–May (MAM), June–August (JJA), and September–November (SON)] precipitation and air temperature at 2 m patterns are presented in Figs. 1a–d and 2a–d, respectively. The patterns are based on gridded data from the Climate Research Unit (CRU) of the University of E. Anglia (Mitchell et al., 2004). The CRU dataset (space resolution of $0.5^\circ \times 0.5^\circ$) is constructed with the use of observation data on a number of climate characteristics made at land stations. Space distributions of precipitation during DJF, MAM, and SON in the EM are significantly controlled by that of the region's topography (Figs. 1a,b,d). Practically no precipitation is found over the southern part of the EM during JJA season (Fig. 1c). The EM conditions fit the “Mediterranean” type according to the Köppen and Geiger's

S. O. Krichak (✉) · J. S. Breitgand · R. Samuels · P. Alpert
Department of Geophysics and Planetary Sciences, Raymond and Beverly Sackler Faculty of Exact Sciences, Tel Aviv University,
Tel Aviv, Israel
e-mail: shimon@cyclone.tau.ac.il

Fig. 1 Observed (CRU) current climate (1961-1990) mean seasonal precipitation (mm) during **a** DJF, **b** MAM, **c** JJA, and **d** SON (*square* in Fig. 1d represents the ECM target area referenced in the following figures)

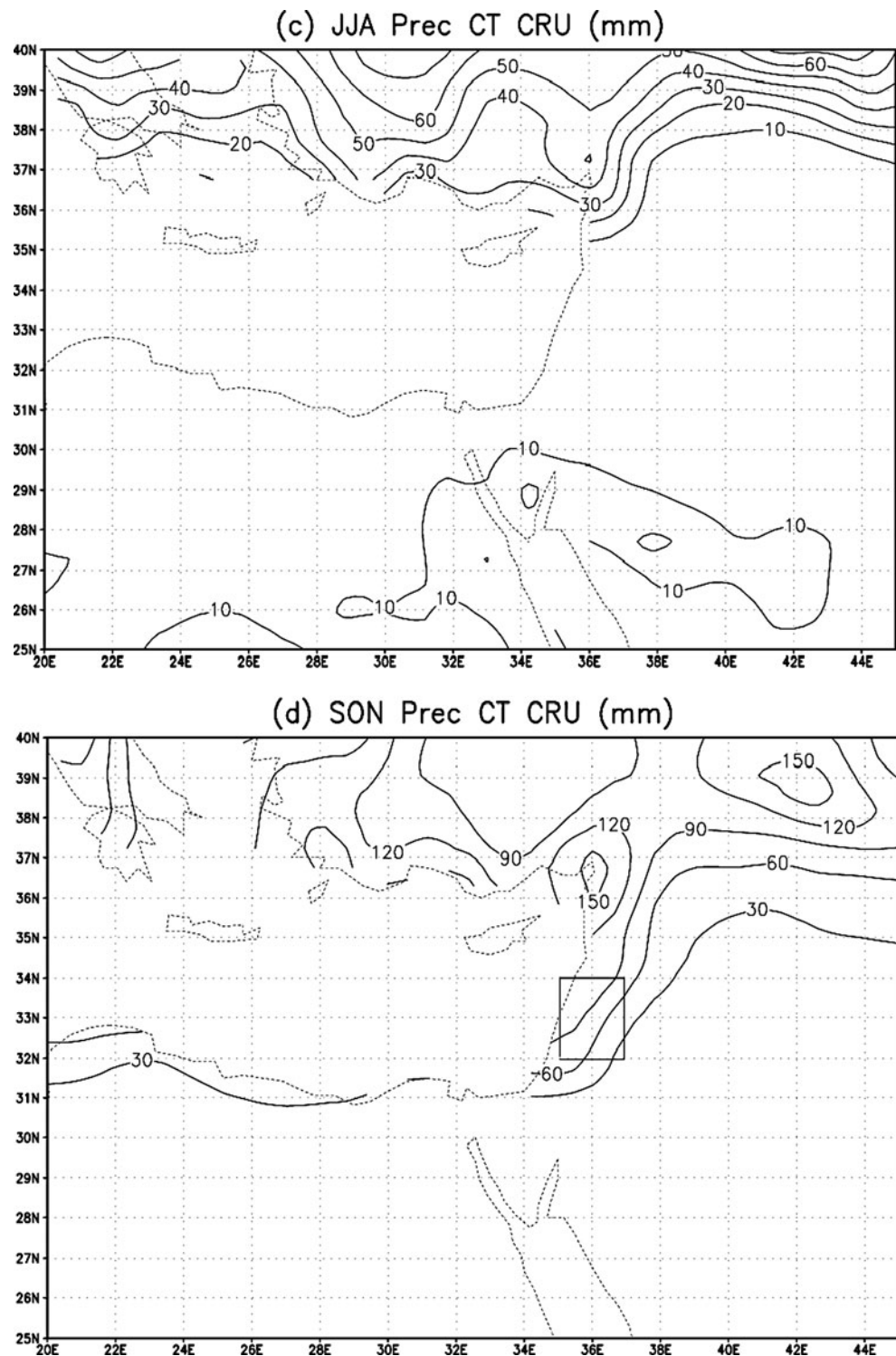


(1936) classification. Patterns with the seasonal distribution of near-surface air temperature also demonstrate the role of the region's topography (Figs. 2a-d). Synoptic processes in the EM are affected by those of mid-latitude and sub-tropical origin. Interannual variations of the region's climate are

controlled by effects of the Hadley cell and Asian-African monsoon circulations (Rodwell and Hoskins, 1996).

Most of the annual precipitation in the EM is produced during a limited number of rainfall events. The EM cyclones are usually associated with upper troposphere

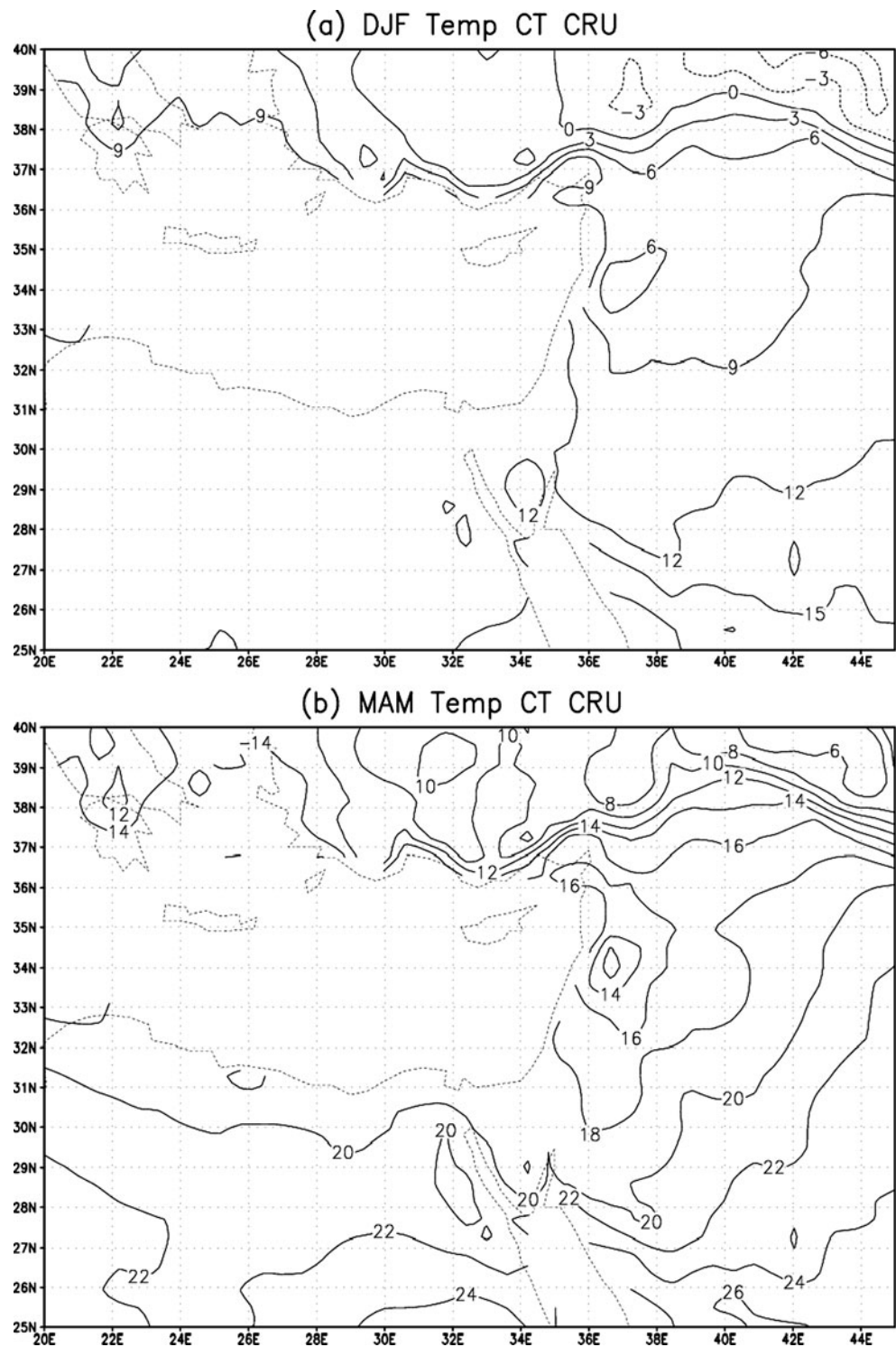
Fig. 1 (continued)



intrusions of cold air masses of north-European origin (Krichak et al., 1997, 2004; Ziv et al., 2005, 2010). Topography and coastal characteristics (with windward effects, gap winds, and land-sea breezes, etc.) also influence the spatial distribution of precipitation patterns in the region

(Krichak et al., 2009a, b). These factors contribute to sharpening gradients in the spatial distributions of the main meteorological variables, especially notable in the mountainous and immediate coastal areas of the EM. Successful descriptions of the mutually interacting effects in the EM

Fig. 2 Same as in Fig. 1, but for 2 m air temperature ($^{\circ}\text{C}$)

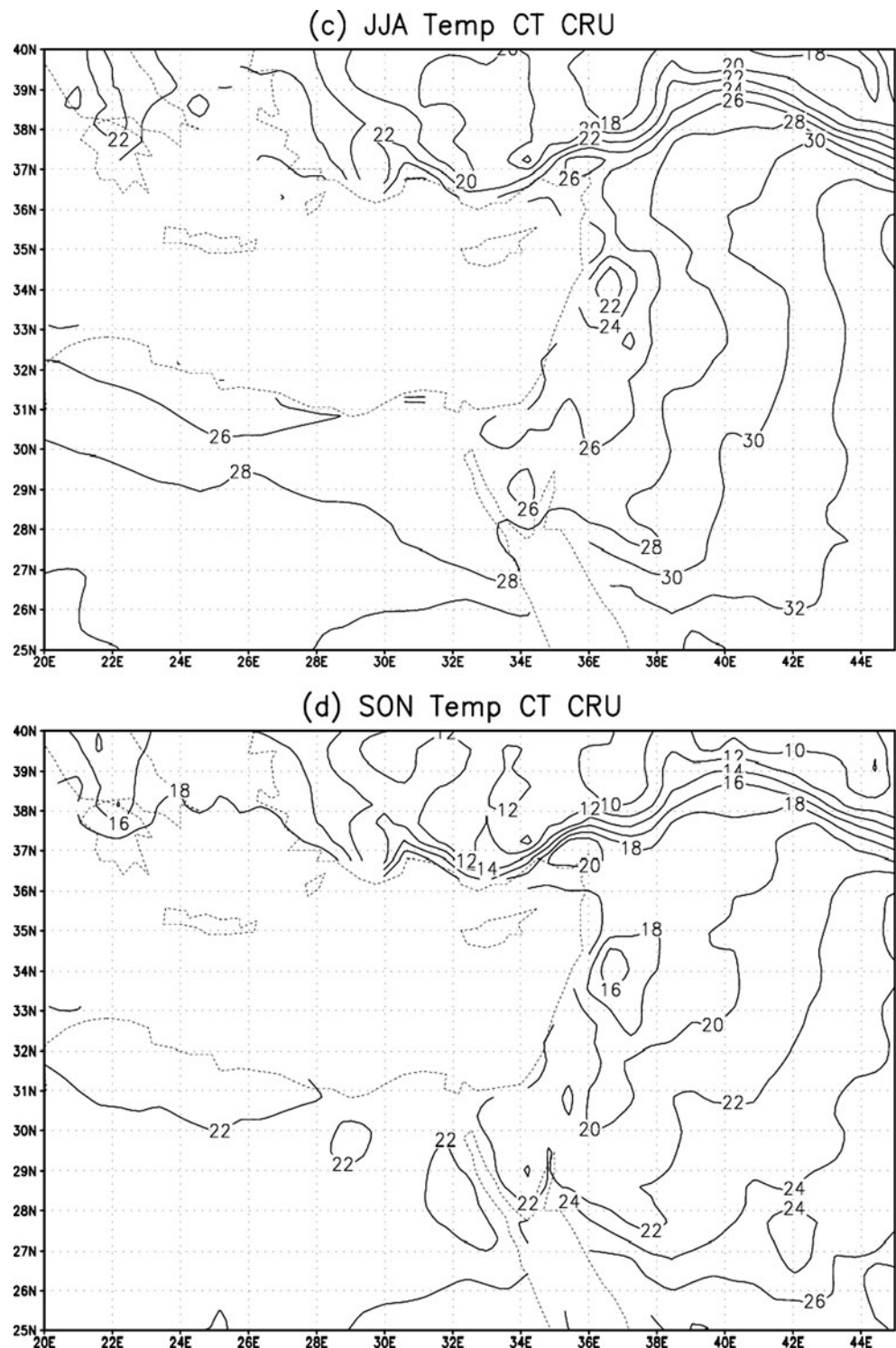


appear necessary for representation of its climate with a RCM.

Most of the past RCM efforts for the EM region have been based on application of a “time slice” approach (i.e., Giorgi et al., 2004a, b). Under this approach, a downscaling

of AOGCM data is performed for two 30-year time periods, representing the current (1961–1990) and future (2071–2100) climates (IPCC 2001). A different, “transient” simulation strategy has been also suggested (IPCC, 2007). The transient RCM simulations are initiated at time

Fig. 2 (continued)

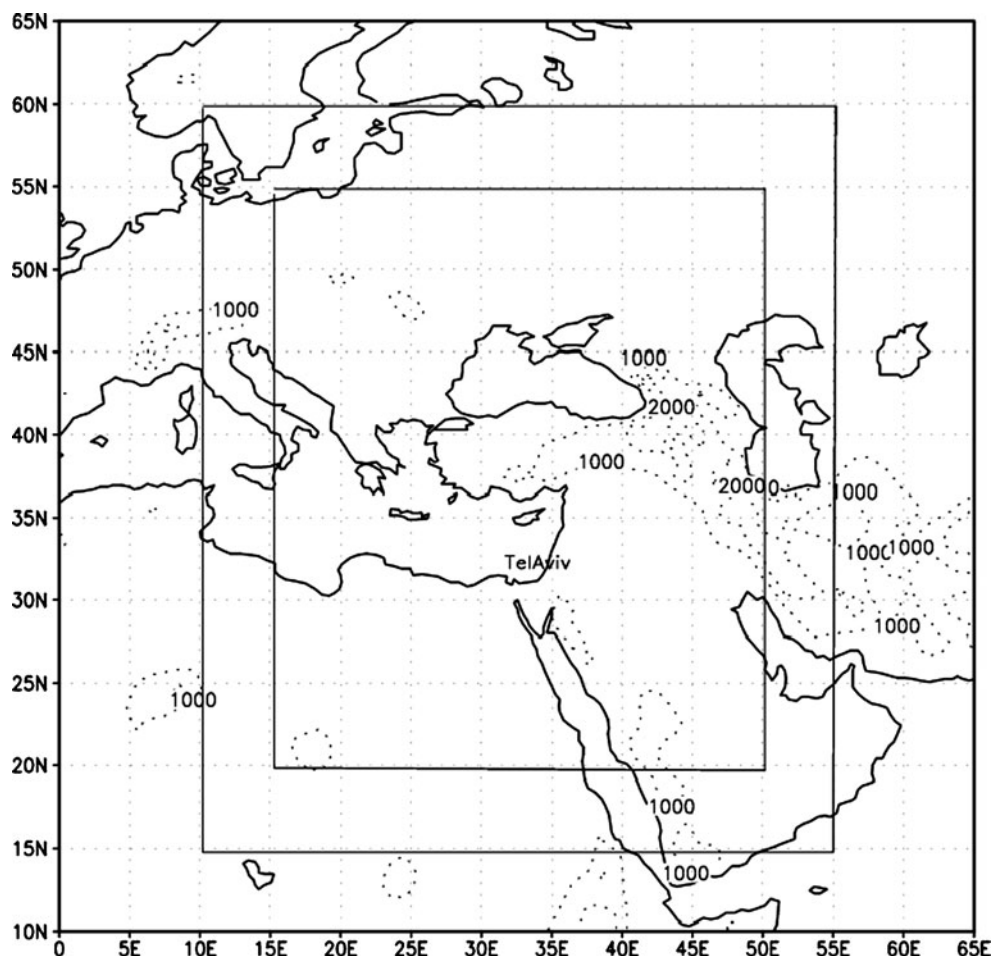


moments corresponding to past climate conditions and are continuously performed to a chosen future date (Hagemann et al., 2008). Under this approach, the high-resolution climate change evaluations are performed based on results for much longer time periods than the 30-year ones adopted under the time-slice strategy. To date, only preliminary

RCM transient simulations of the EM climate change have been reported (Heckl and Kunstmann, 2009; Krichak et al. 2009a, b; Onol, 2008).

The current paper presents results of a RCM effort focused on determination of the climate change projections for the EM region during the first half of 21st century using

Fig. 3 Simulation domain (inner square represents the area not affected by the lateral boundary relaxation procedure)



an optimally configured RCM model RegCM3 (Giorgi et al., 2004b; Krichak et al. 2009a, b; Pal et al., 2007). A double resolution transient climate change simulation of anthropogenically induced climate change processes over the EM is performed; projections of the regional climate change trends of several climate parameters are determined and evaluation of the role of the physical mechanisms involved is undertaken. The experimental setup is discussed in Section 2. Results of simulations of the current climate conditions over the EM region are presented in Section 3. The issue of sensitivity of the simulated climate projections to smaller scale effects is addressed in Section 4. The obtained projections of the EM climate to the middle of the 21st century are presented in Sections 5. Discussion of the results is given in Section 6.

2 Methodology of analysis and experiment setup

The RCM model used is the third generation RegCM3 model (Pal et al., 2007) of the International Center for Theoretical Physics (ICTP). Two sets of the RCM simu-

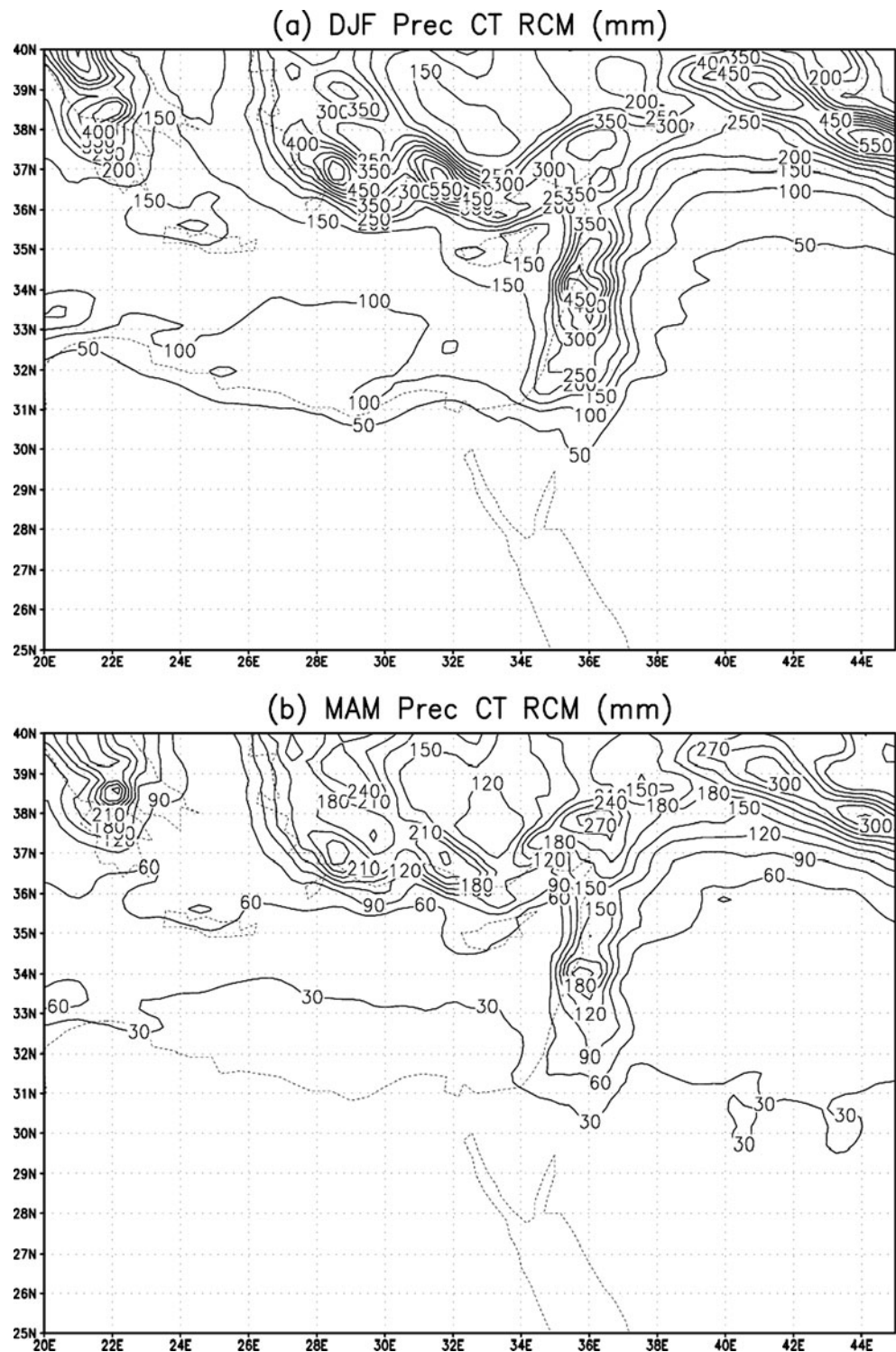
lations are realized with 50 km and 14 vertical (50 km/14 L) levels and 25 km and 18 vertical levels (25 km/18 L) space resolutions (Krichak and Alpert, 2010). The top of the model’s atmosphere is defined at 80 hPa. The model domain used covers southern Europe, the eastern part of the Mediterranean region, and the Middle East (Fig. 3). The size and configuration of the model domain have been selected to allow a representation of main synoptic processes

Table 1 Area-averaged (36–39°E; 32–36°N) multi-year (1961–1990) differences between model-simulated and CRU data for air temperature at 2 m (°C) and precipitation (mm)

		DJF	MAM	JJA	SON
PREC	RCM50-CRU	7.7	−19.9	−2.9	−1.6
	RCM25-CRU	0.7	−4.9	−0.2	2.6
T2m	RCM50-CRU	−0.1	−0.3	−0.3	1.1
	RCM25-CRU	0.6	0.6	−0.3	1.1

Area-averaged (36–39°E, 32–36°N) multi-year (1961–1990) differences between model-simulated and CRU data for monthly mean air temperature at 2 m (°C) and precipitation (mm)

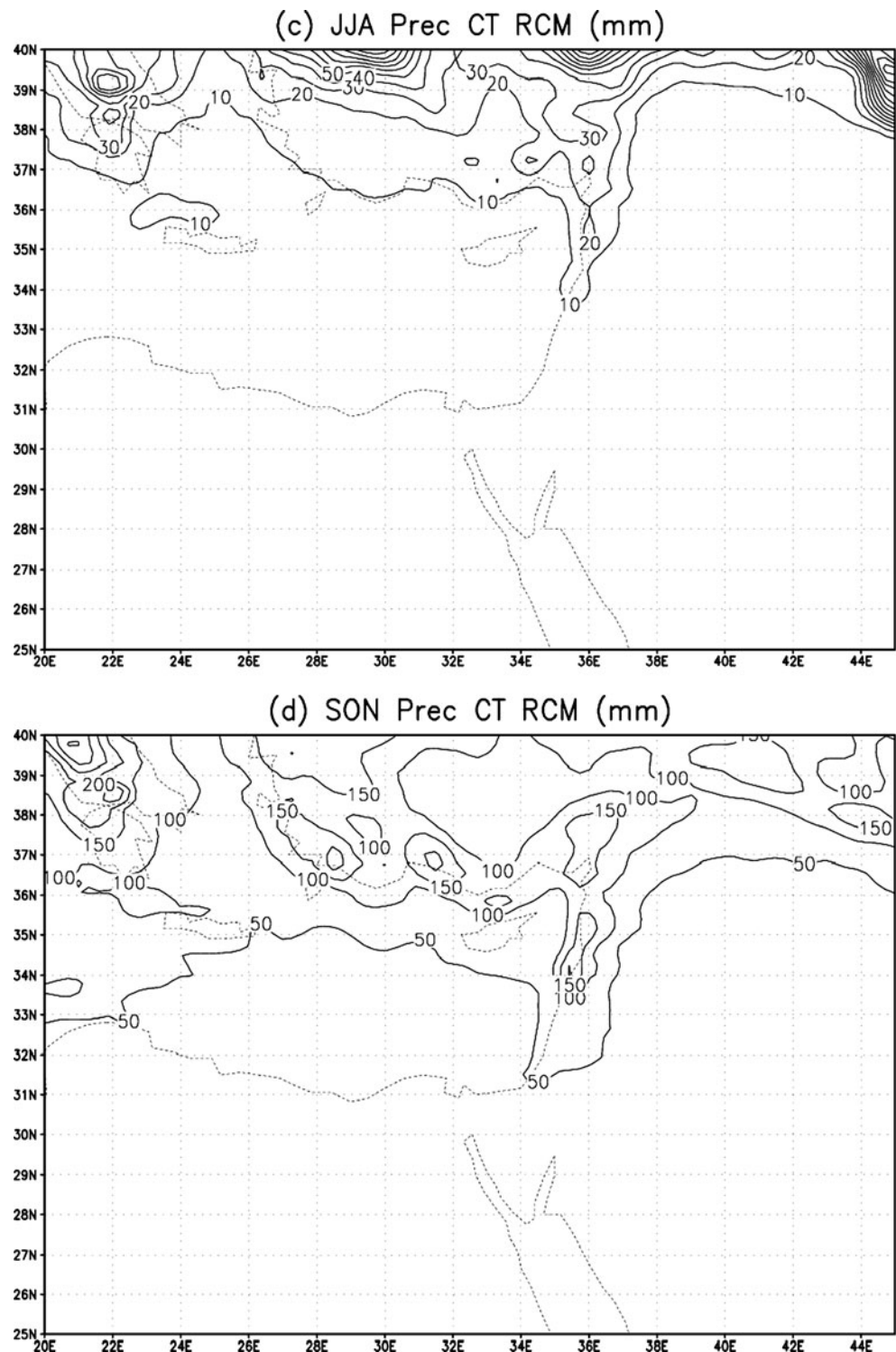
Fig. 4 Same as in Fig. 1, but for RCM results from the 25 km/18 L experiment



important for description of the EM climate (Krichak et al. 2009b). The domain includes 160×160 grid points (25 km resolution) and 80×80 grid points (50 km). The inner square in Fig. 3 represents the sub-domain in which variation of the model's history variables are hydrodynamically determined

during the simulation experiment. The outer part of the domain corresponds to the relaxation zone at which lateral boundary computations are performed. The physical options used are discussed separately (Krichak et al. 2007, 2009a, b; Krichak 2008; Samuels et al. 2009).

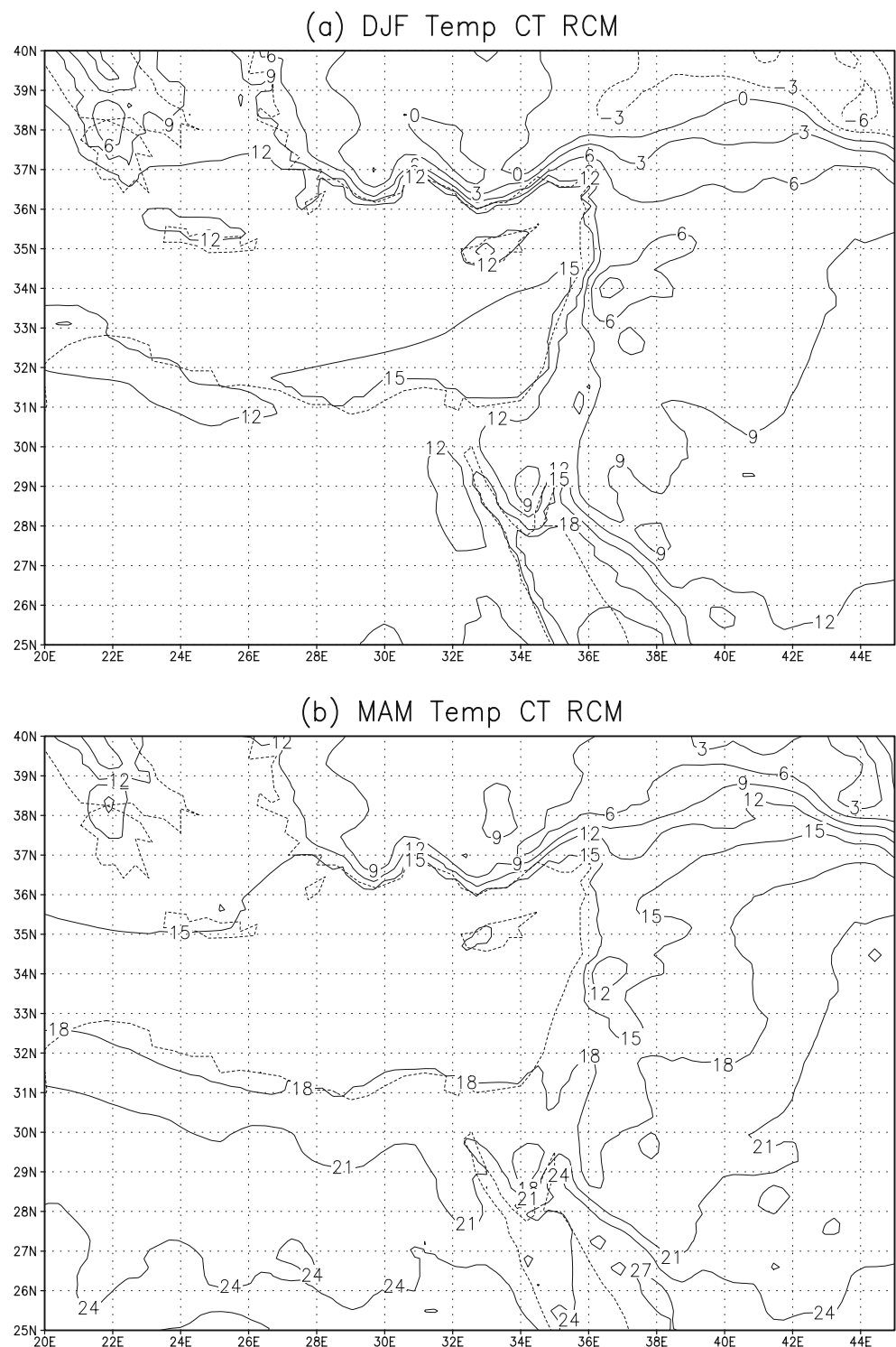
Fig. 4 (continued)



The driving data adopted are from a transient climate change simulation experiment performed with the fifth-generation global atmosphere-ocean ECHAM5/MPI-OM model of the MPI-M (Muller and Roeckner, 2008). The ECHAM5 atmosphere model is hydrostatic with spectral

T63 truncation (1.875×1.875 spatial resolution) and 31 hybrid vertical levels. The ocean model MPI_OM uses a conformal mapping grid with a horizontal grid spacing of 1.5° and 40 vertical levels. The ECHAM5/MPI-OM experiment is initiated from the pre-industrial period

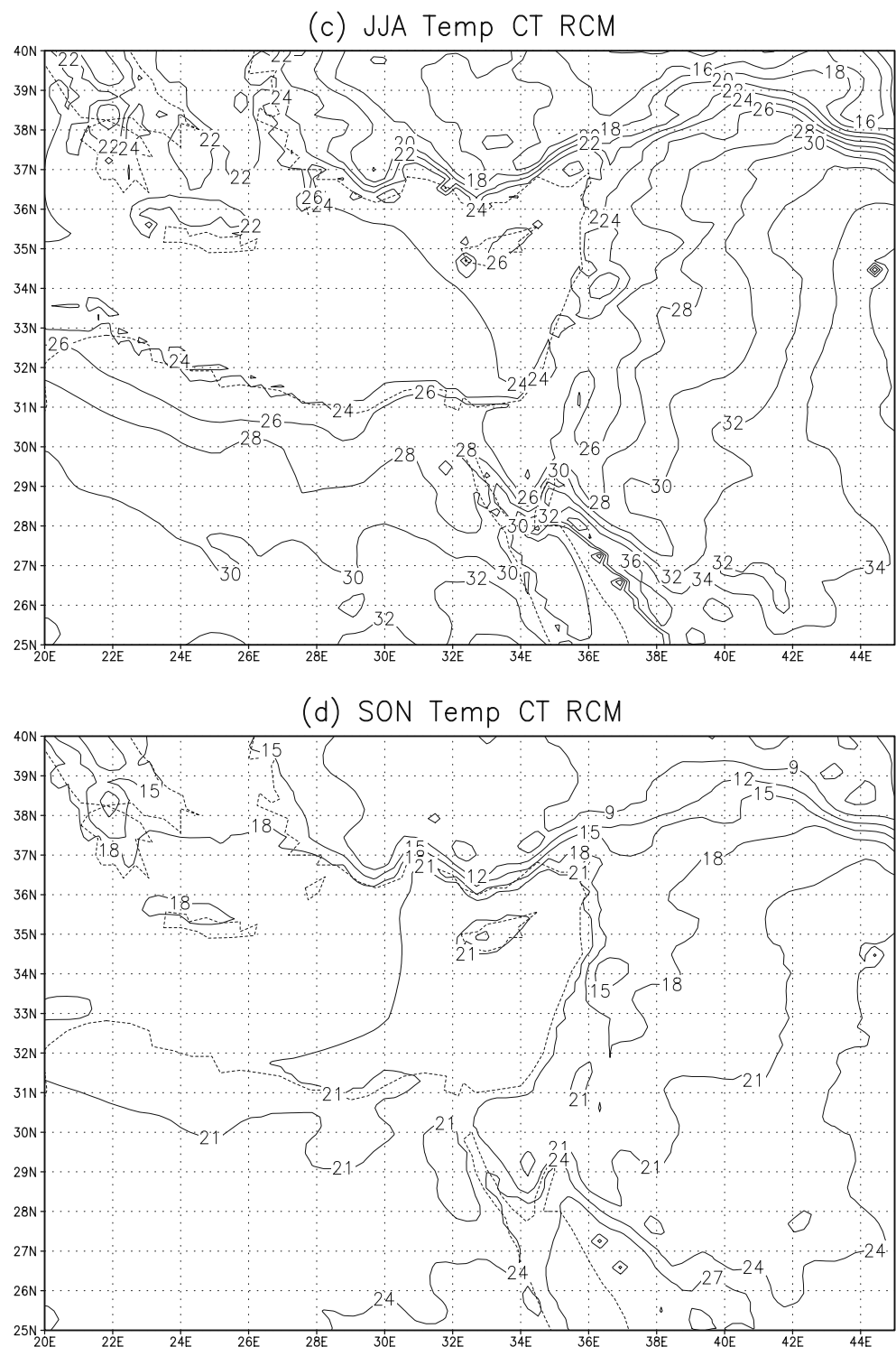
Fig. 5 Same as in Fig. 2, but for RCM results from the 25 km/18 L experiment



(~1,850). For the future climate projection, the ECHAM5 experiment employed greenhouse gases (GHG) emission scenario A1B (IPCC 2001). Within the full range of the IPCC GHG anthropogenic emission scenarios, the A1B scenario (IPCC 2007; Raupach et al., 2007) predicts a

medium-high increase of CO_2 concentration to about 700 ppm by 2100 with carbon emissions ranging from between 1,450 and 1,800 GtC. The mixing of the CO_2 into the deep ocean maintains a slow surface ocean CO_2 increase, so in A1B the oceanic sink steadily increases.

Fig. 5 (continued)



Also in A1B, fossil fuel emissions increase until 2050 and decrease thereafter.

As opposed to some other regions in the world, the future climate change projections based on results of multiple Fourth Assessment Report of the Intergovernmen-

tal Panel on Climate Change (AR4 IPCC) are fairly consistent when it comes to the region of the Mediterranean where annual precipitation and number of rainy days are likely to decrease and temperatures, especially those in the summer are likely to increase (IPCC, 2007). When

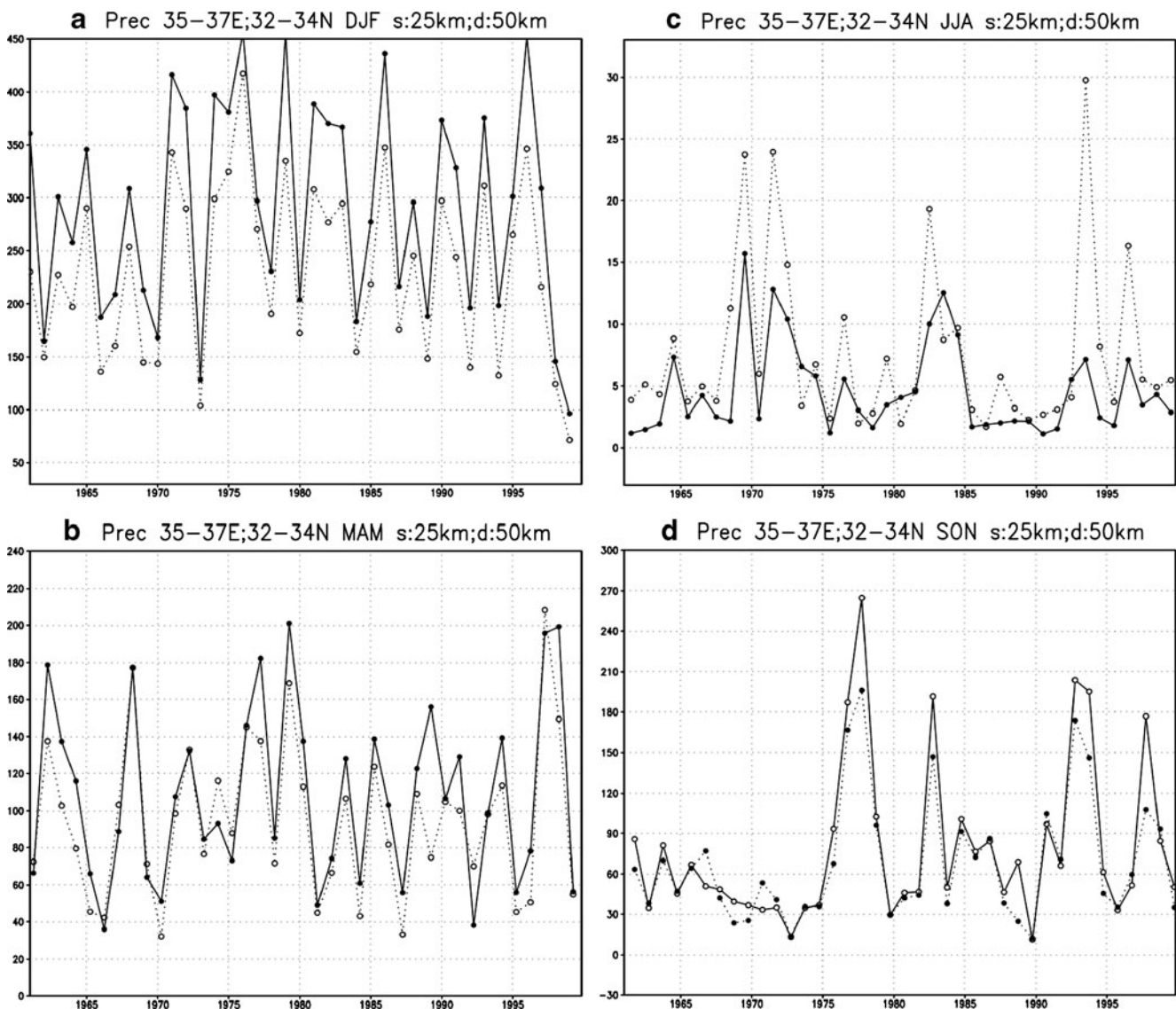


Fig. 6 Area average of the monthly precipitation (mm) the ECM target area (indicated in Fig. 1d) during 1960–2000 as simulated RCM experiments with 25 km/18 L (*solid*) and (50 km/14 L) space resolutions **a** DJF, **b** MAM, **c** JJA, **d** SON

compared with the other IPCC AOGCM results, results of the ECHAM5 model used to drive the RegCM show a slower drying than than produced by most of the models from the 2020–2040 time period. The trend is caught up by the experiment in the later decades (2040–2060 and later; e.g., Samuels et al. 2009).

3 Simulation of the current climate

3.1 Spatial distribution of seasonal precipitation and air temperature

Parameters of the current EM climate as produced by the experiment are discussed in this section. The results are

presented separately for four (DJF, MAM, JJA, and SON) seasons. To evaluate the level of success of EM climate representation by the model, multiyear seasonal means of the simulated results are compared with those from the CRU archive. Table 1 presents multiyear (1961–1990) mean absolute differences between the total precipitation and air temperatures at 2 m (T2m) from the model run and the CRU archive averaged over a large Middle East sub-area (36°E–39°E; 32–36°N). As follows from the table, the use of 25 km (instead of 50 km) horizontal resolution allows for a significant improvement of the RCM results over the sub-area for precipitation during the four seasons. Less notable is the contribution of higher space resolution to the accuracy of representation of the air temperature distribution over the

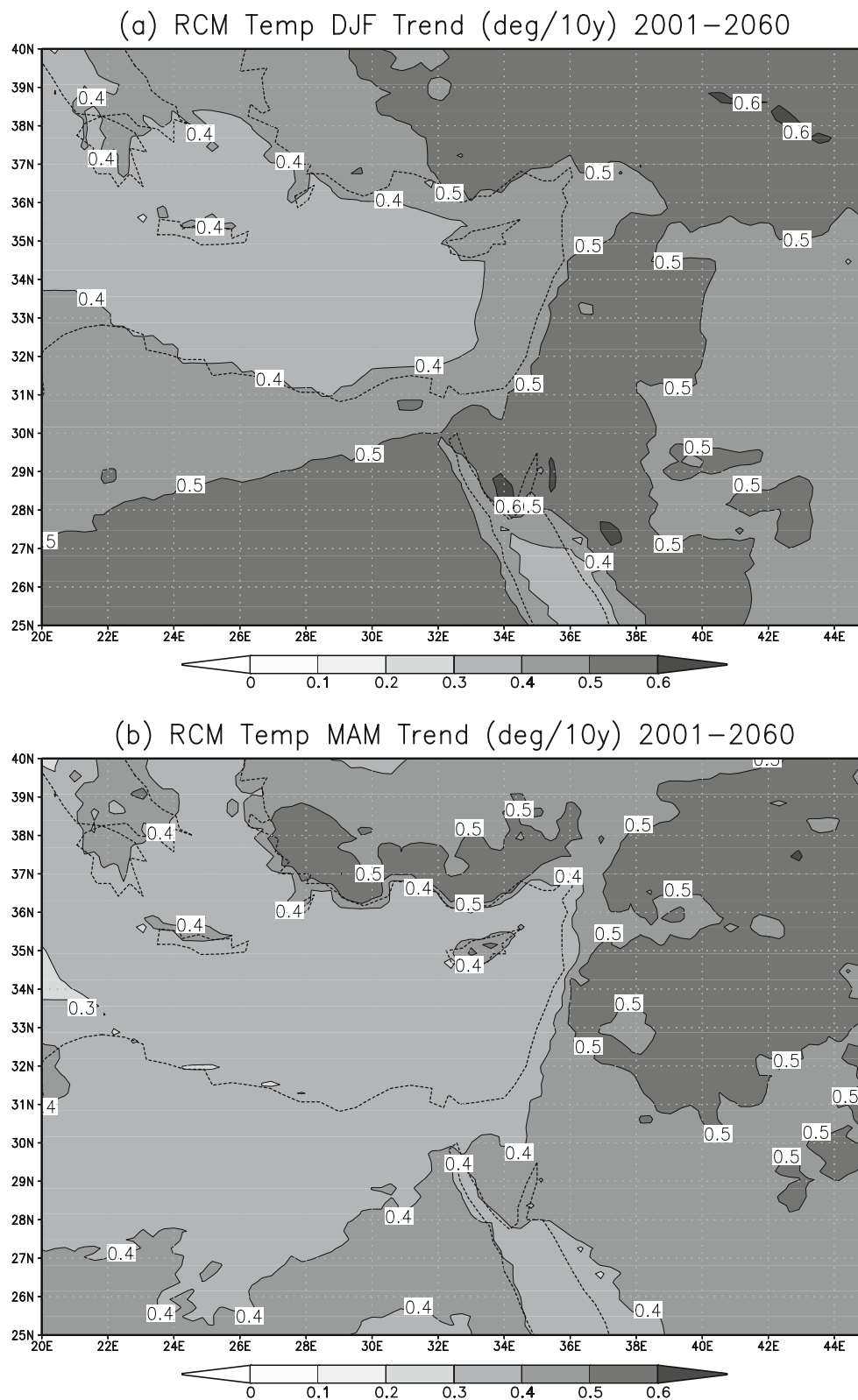


Fig. 7 Same as in Fig. 6, but for 2 m monthly air temperature ($^{\circ}\text{C}$)

sub-area. As is demonstrated in the following, the use of the higher-resolution allows a more accurate RCM representation of the air temperature in the near-coastal zone however.

DJF, MAM, JJA, and SON patterns with the simulated precipitation and T2m fields averaged for 1961–1990 are given in Figs. 4a–d and Fig. 5a–d, respectively. The patterns may be compared with those in Fig. 1a–d and Fig. 2a–d.

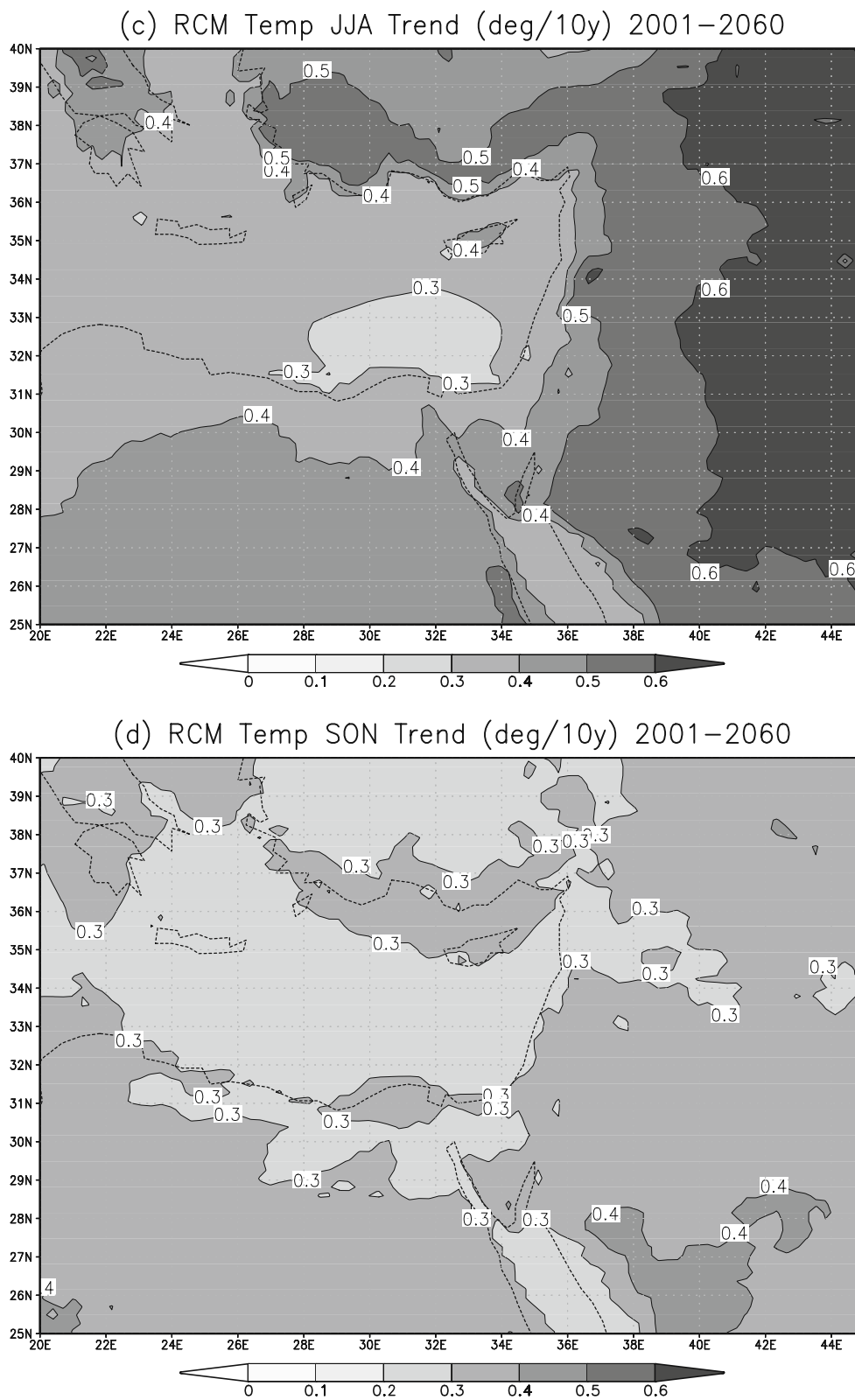
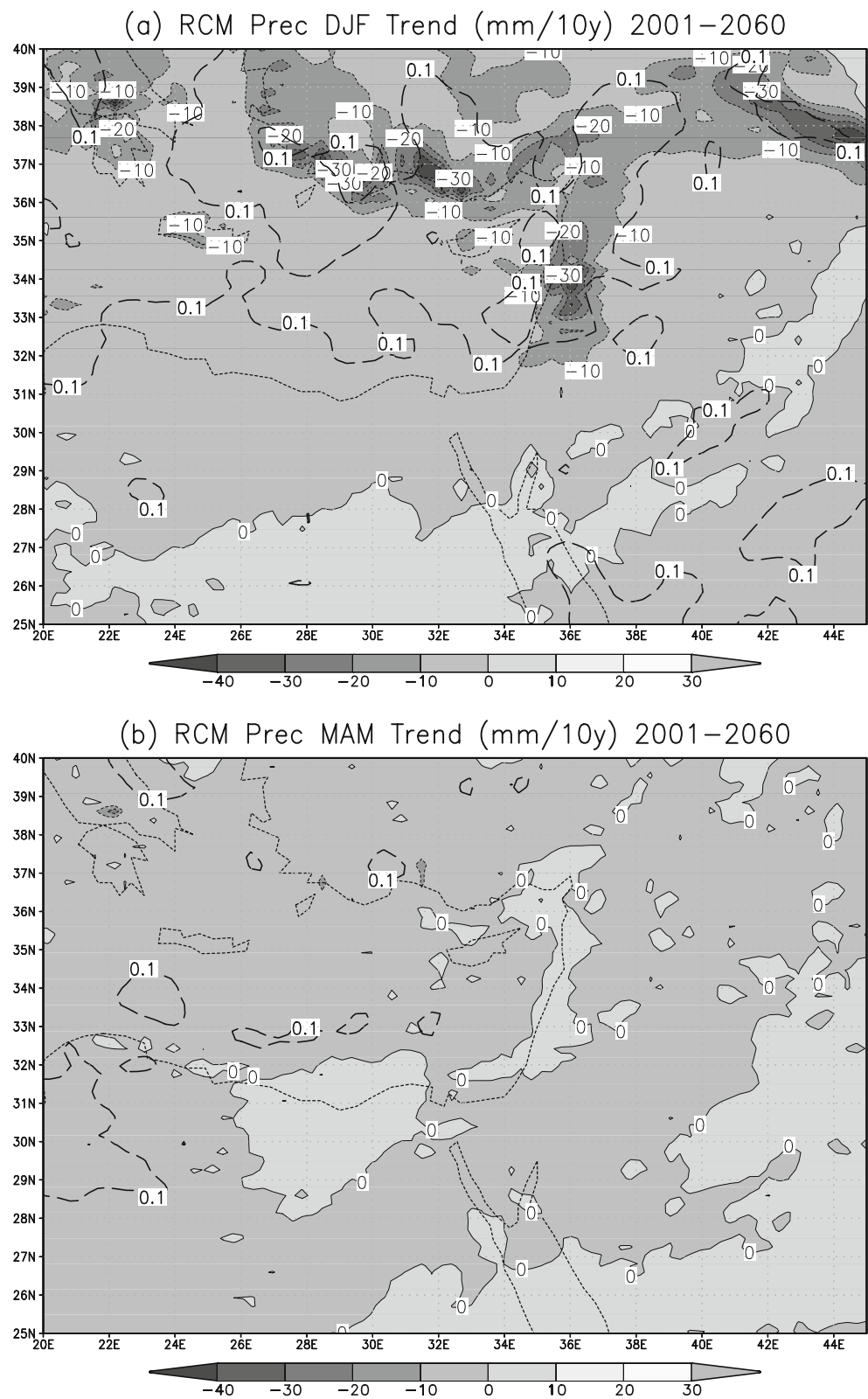


Fig. 7 (continued)

The areas that have little or no precipitation in Fig. 4a-d are well located even at some relatively small scales; however, there is a tendency for the model to simulate excessive

precipitation over some of the steep mountainous areas. This is clear in the patterns for DJF (Figs. 1a, 4a), although is less evident in the pattern for MAM (Figs. 1b, 4b) and

Fig. 8 Linear trend in seasonal precipitation (mm) **a** DJF, **b** MAM, **c** JJA, **d** SON (*black solid lines* indicate zones with 90% significance level of the trend)

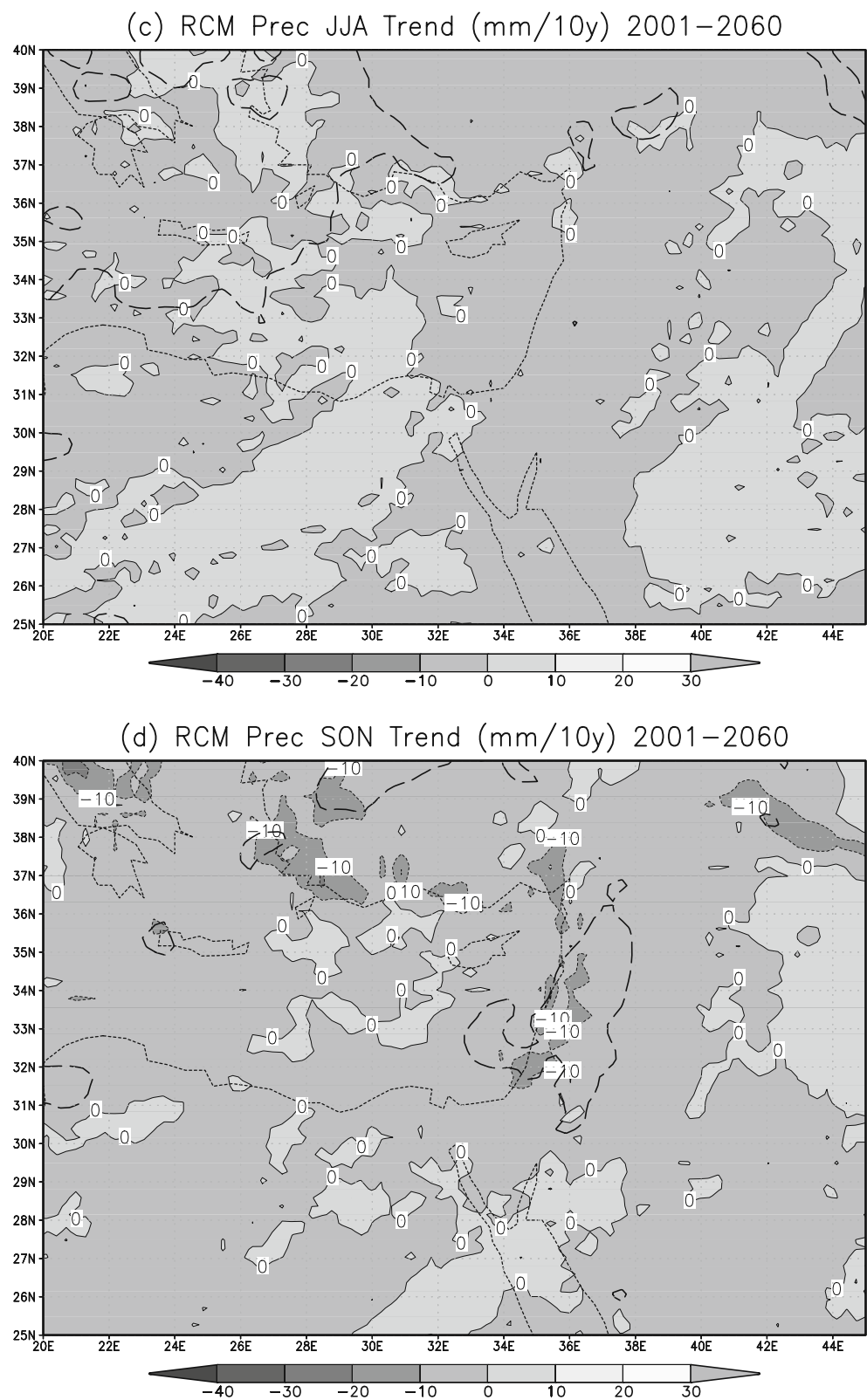


SON (Figs. 1d, 4d). It should be also noted that the CRU data are available at a much coarser resolution ($2\times$) than that of the model (25 km). This might be part of the explanation for the discrepancy between the simulated and

CRU current climate precipitation, especially over data sparse areas.

The modeling results also provide reasonably successful representations of mean seasonal 2 m air temperature

Fig. 8 (continued)

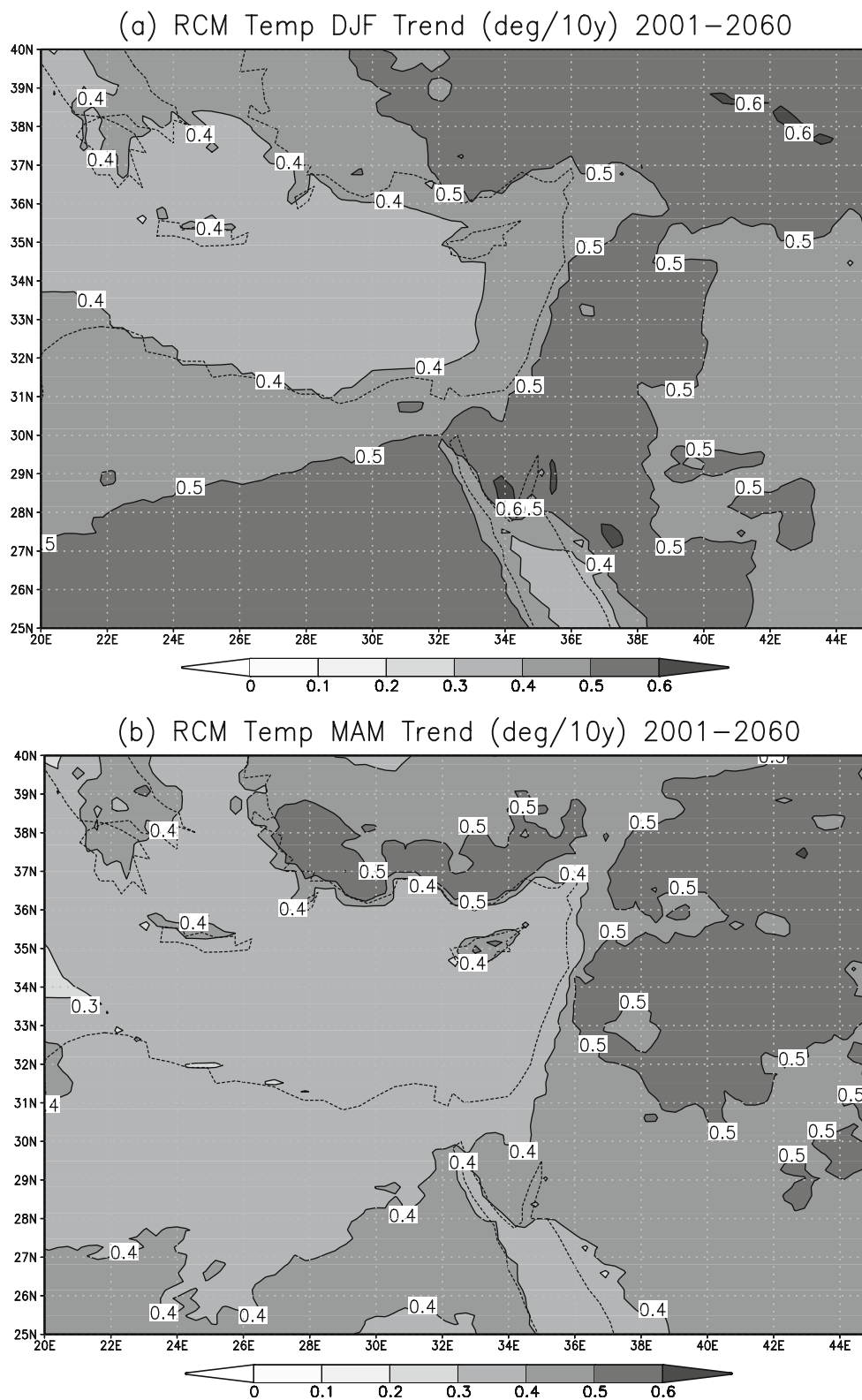


patterns for DJF, MAM, JJA, and SON (Fig. 5a-d). Over most of the southern EM, the model shows a tendency to slightly overestimate temperature. In summary, the 25 km/18 L RegCM3 performs well in simulating the

precipitation and low-level/surface temperature, over the area.

Discussed above peculiarities of the current EM climate (including those in temperature and precipitation) are

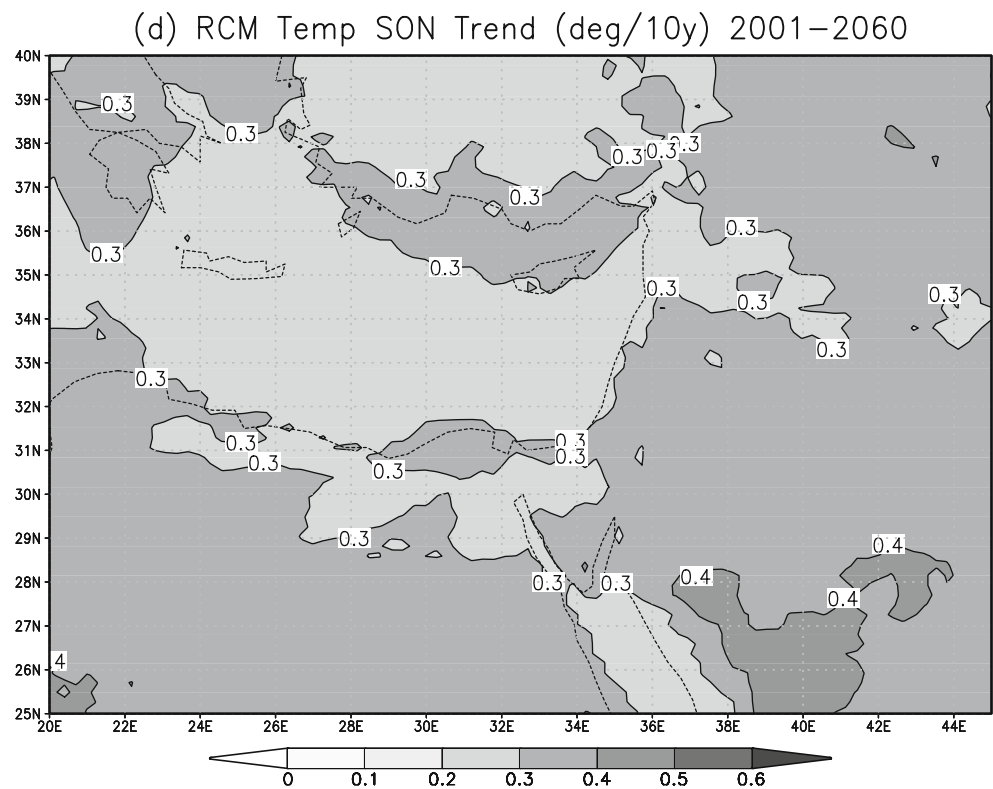
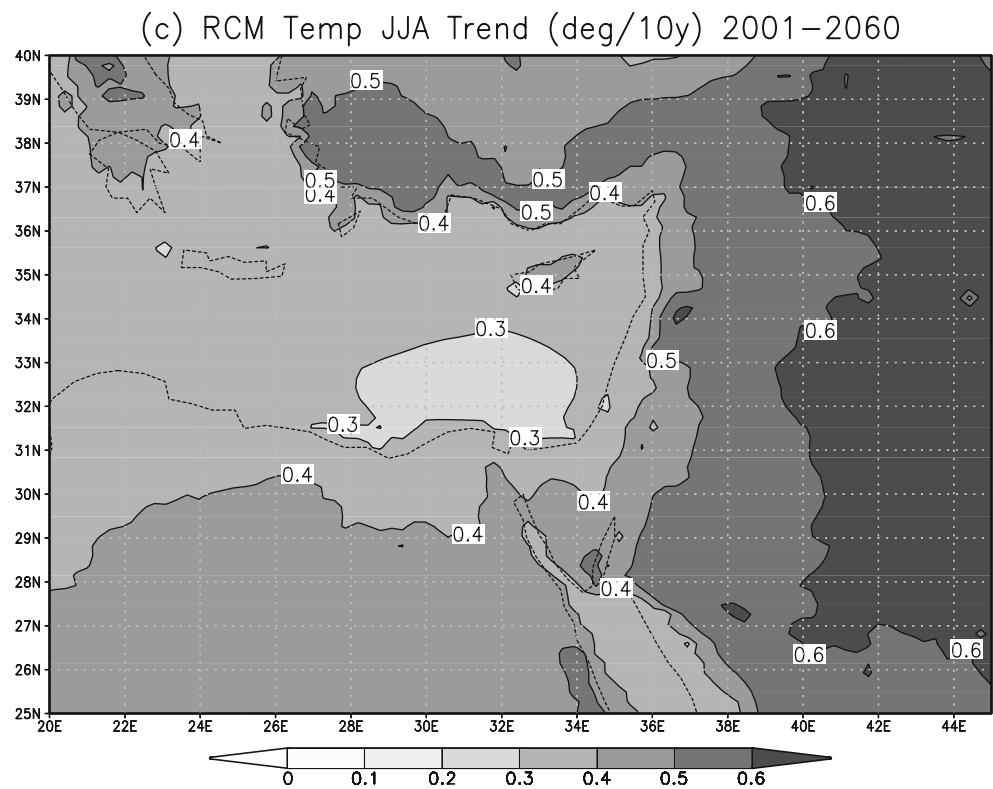
Fig. 9 Same as in Figs. 8 but for 2 m monthly air temperature (°C; 95% significance level over the whole area)



reasonably represented in the both 50 km/14 L (see also Krichak et al. 2009a; Samuels et al. 2009) and 25 km/18 L simulation runs. Some differences, representing the contribution of smaller scales, are detectable however. An

evaluation of the differences is performed below to determine the sensitivity of the simulated climate and climate change trends in the region to the effects of the smaller spatial scales.

Fig. 9 (continued)



3.2 Time variability of simulated climate parameters

The RCM effort presented is specifically focused on simulation of climate and its projected changes over north

Israel and adjacent areas in the southeastern Mediterranean coastal zone, hereafter ECM). With this aim, an ECM target area (35–37°E; 33–36°N) has been defined for further evaluations (indicated by square in Fig. 1d). This area is

considered important for water resources and agricultural production in the highly populated region of Israel making it very vulnerable to expected climate change (e.g., Samuels et al. 2009). To evaluate the sensitivity of the simulated climate to the model spatial resolution, area-averaged monthly mean precipitation and near-surface temperature produced for the years 1960–2000 for the target area at 50 km (dotted line) and 25 km (solid line) resolutions were calculated. Results from simulations are presented in Fig. 6a–d (precipitation) and Fig. 7a–d (temperature). No time averaging of the data series is performed to keep the time variability unchanged. As above, the time series are aggregated separately for four seasons (DJF, MAM, JJA, and SON).

The joint presentation of the 25 and 50 km results allows for an evaluation of the contribution of smaller

scale effects in the RCM simulation over the region. During DJF, MAM, and SON (Fig. 6a,b,d), the 25 km experiment produces systematically higher amounts of precipitation over the ECM than the 50 km one while precipitation amounts for JJA season are notably lower (Fig. 6c). When compared with observed trends, the results of the 25 km experiment with higher precipitation in the winter and lower precipitation during the summer are more accurate than the corresponding 50 km results. According to Fig. 7a–d, the use of higher (25 km/18 L) space resolution leads to a 1.0–1.5°C decrease in the seasonal T2m calculated for DJF, MAM, and SON (Fig. 7a,b,d). At the same time, the area averaged air-temperature simulated in the 25 km experiment for JJA (Fig. 7c) seasons over the ECM are slightly

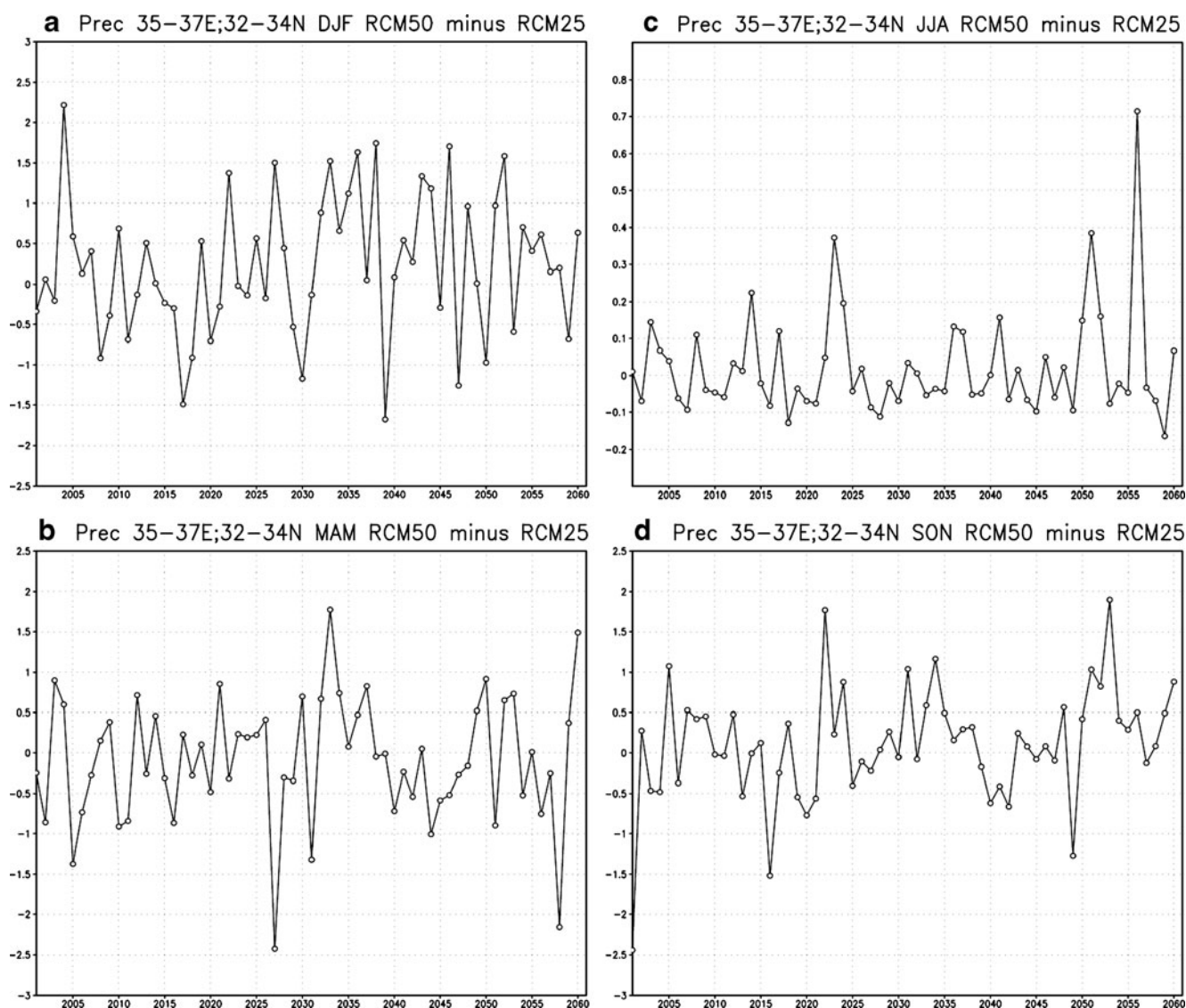


Fig. 10 Time variation of area averaged difference in mean seasonal precipitation over the ECM simulated in the 50 km/14 L and 25 km/18 L RCM experiment **a** DJF, **b** MAM, **c** JJA, **d** SON

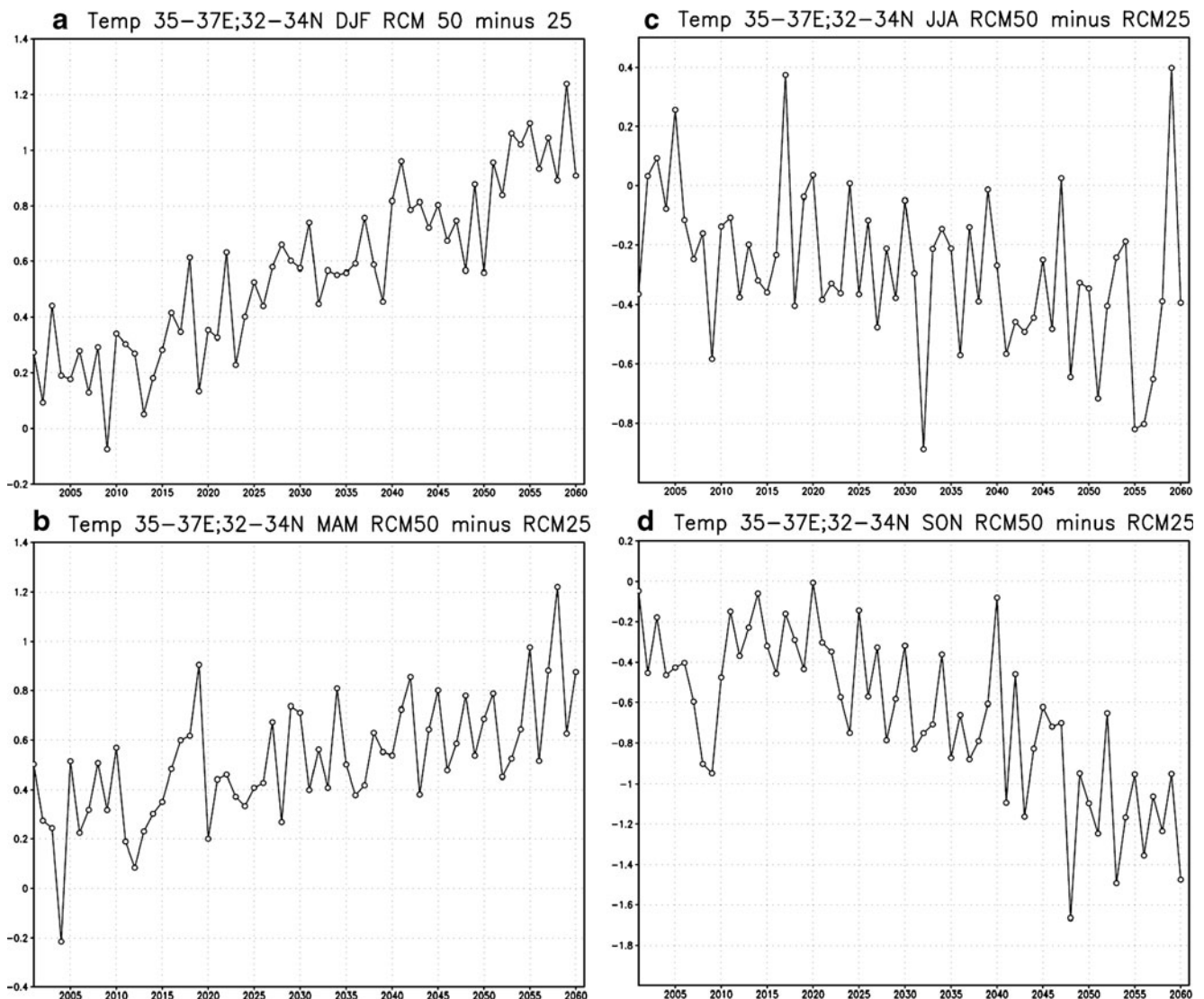


Fig. 11 Same as in Figs. 10 but for 2 m monthly air temperature ($^{\circ}\text{C}$)

($0.2\text{--}0.3^{\circ}\text{C}$) higher, than those produced in the 50 km run.

Comparison between the simulated and observed precipitation and air temperature fields between model results and CRU data shows that the high-resolution RegCM3 skillfully captures the general climate rainfall patterns during the four seasons. In accordance with this, the following discussions are mainly based on data from the 25 km/18 L RCM run.

4 Projection of future changes of the ECM climate

Climate parameters from the RCM simulations are characterized by oscillations of different time-scales. The oscillations of regional climate parameters at

relatively short-time (several years) scales are to a large extent a reflection of the nonlinear and chaotic nature of the real climate system and apparently have no (or very little) predictability (Giorgi 2005). Relatively long-term (inter-decadal) regional trends are due to a mixture of natural and computational factors: the nonlinear nature of the climate system, the regimes of the general circulation of the coupled atmosphere-oceans system, the presence of feedback and threshold processes (Rial et al, 2004), effects of model internal variability (e.g., Caya and Biner, 2004), etc. The trends up to some extent may be representing contributions of physically meaningful climate change processes taking place both inside and outside of the region (Gubasch, 2001; Leckebusch and Ulbrich, 2004; Meehl et al., 2000; Ulbrich and Christoph 1999).

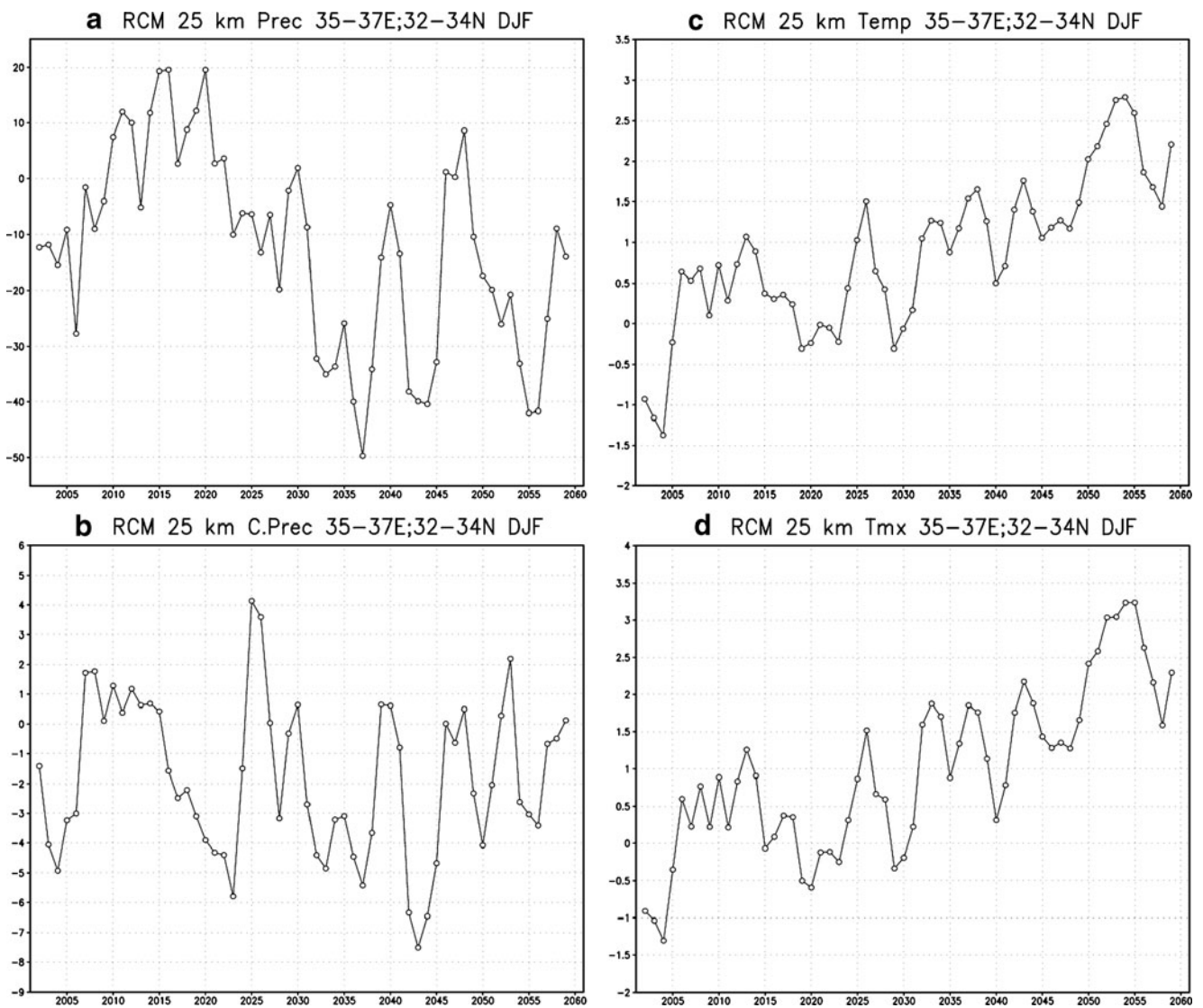


Fig. 12 Time variation in area averages climate change variations of monthly mean parameters over the ECM target area during DJF as simulated by RegCM3 (25 km/18 L) for **a** precipitation (mm), **b** convective precipitation (mm), **c** temperature ($^{\circ}\text{C}$ at 2 m), **(d)**

temperature maximum ($^{\circ}\text{C}$ at 2 m), **e** temperature minimum ($^{\circ}\text{C}$ at 2 m), **f** relative humidity (% at 2 m), **g** maximum wind speed (m s^{-1} at 10 m), **h** solar incident flux (Wt m^{-2})

4.1 Linear trends

In addition to the time varying signal however, the experiment also exhibits climate trends persisting during the simulation period. Climate variability of this type is affected by anthropogenic forcings and may be considered representative of the climate change signals (Giorgi, 2005). As a first step for determination of the anthropogenically induced climate change variations, least-square linear trends in the simulations for multi-year seasonal precipitation and near-surface air temperature were computed. Significance of the linear trend (slope) has been tested against the zero trend according to Mann-Kendall method

(Kendall and Dickinson Gribbons, 1990; Mann, 1945). Figures 8a-d, 9a-d present the computed linear trends for precipitation and air temperature performed at every grid point starting from the yearly seasonal data. Zones with significance at 90% level linear trends in precipitation are indicated by solid black contours in Fig. 8a-d. No such contour lines are found in Fig. 9a-d since linear trends in near-surface air temperature are characterized by significant trends over the whole area. The trends for the both parameters are displayed on a latitudinal-longitudinal plot to yield a two-dimensional trend distribution. Figures 8a-d present linear trends in the seasonal precipitation (millimeter per decade) during DJF, MAM, JJA, and SON,

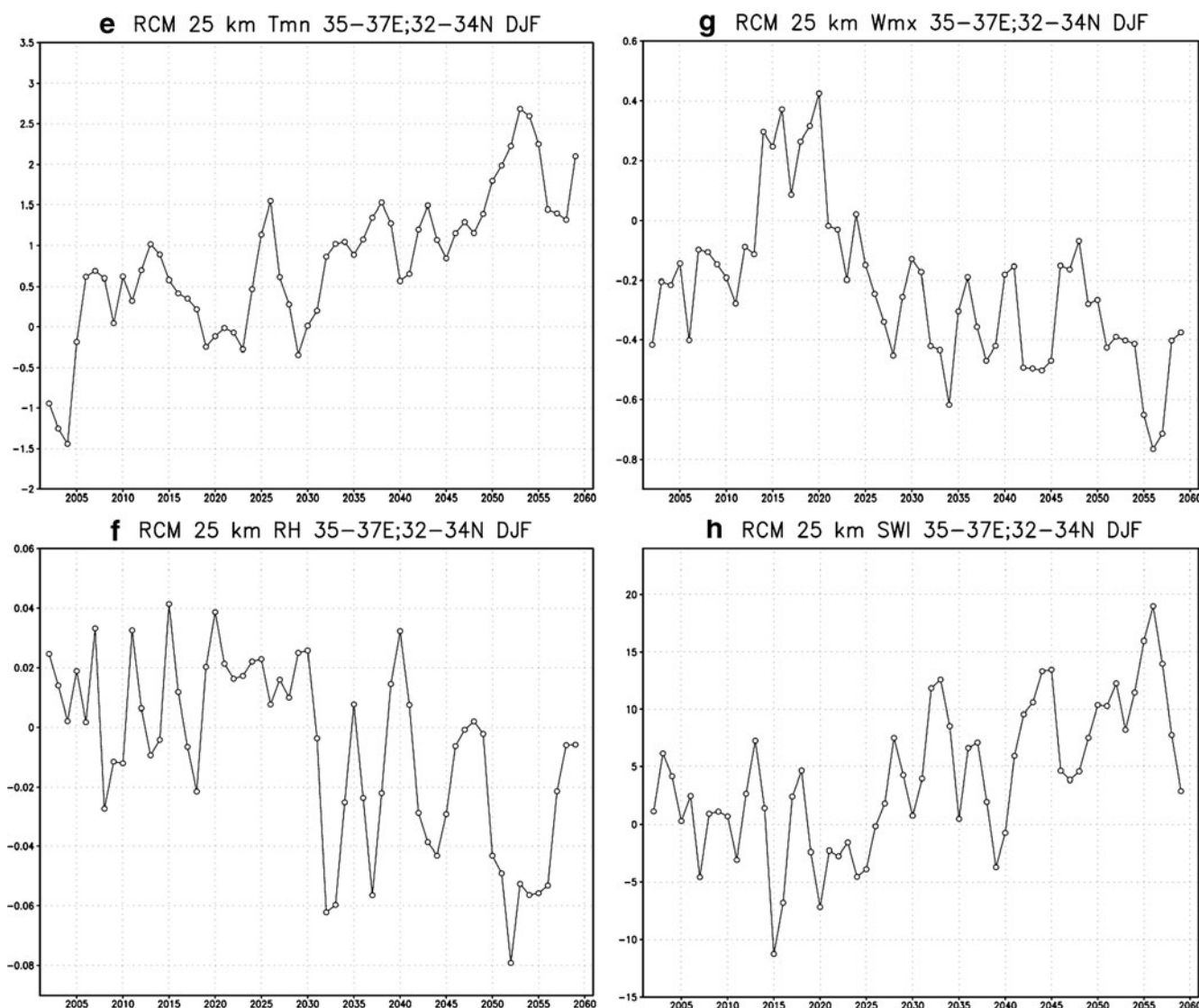


Fig. 12 (continued)

respectively, over the 60 year period 2001–2060. The near-coastal zone of the EM region is characterized by a notable trend to decline in precipitation during DJF winter seasons (Fig. 8a). A significant drop in precipitation reaching ($-30 \text{ mm decade}^{-1}$) is projected for the ECM. Similar changes in seasonal precipitation amount are projected for the northern part of the EM. A minor negative trend ($10 \text{ mm decade}^{-1}$) characterizes northern parts of the EM during spring (MAM). A minor (and non-significant) rise in MAM precipitation amount (5 mm decade^{-1}) is projected for the ECM (Fig. 8b). Practically no changes in precipitation amount are projected for the whole EM region during summer (JJA) (Fig. 8c). The RCM experiment projects less notable decreases than in the winter but also a negative significant precipitation

trend (down to $\sim 10 \text{ mm decade}^{-1}$) during autumn (SON) (Fig. 8d) over the EM coastal zone.

The linear trends in air temperature at 2 m over the EM are given in Figs. 9a–d. The whole region is characterized by significant T2m trends. A $0.4\text{--}0.5^\circ\text{C decade}^{-1}$ air temperature rise is projected for winter (Fig. 9a). A slightly less intense warming process is projected for the EM region during spring (Fig. 9b) with a warming is of $\sim 0.3^\circ\text{C decade}^{-1}$ over the coastal zone (including the ECM). A more intense warming ($0.5^\circ\text{C decade}^{-1}$) characterizes continental regions in southern part of Asia Minor and northeastern Mediterranean. Also, relatively slow T2m 60 y rise ($0.35^\circ\text{C decade}^{-1}$) is projected over the near coastal central EM zone (including the ECM) during summer (JJA; Fig. 9c). The warming

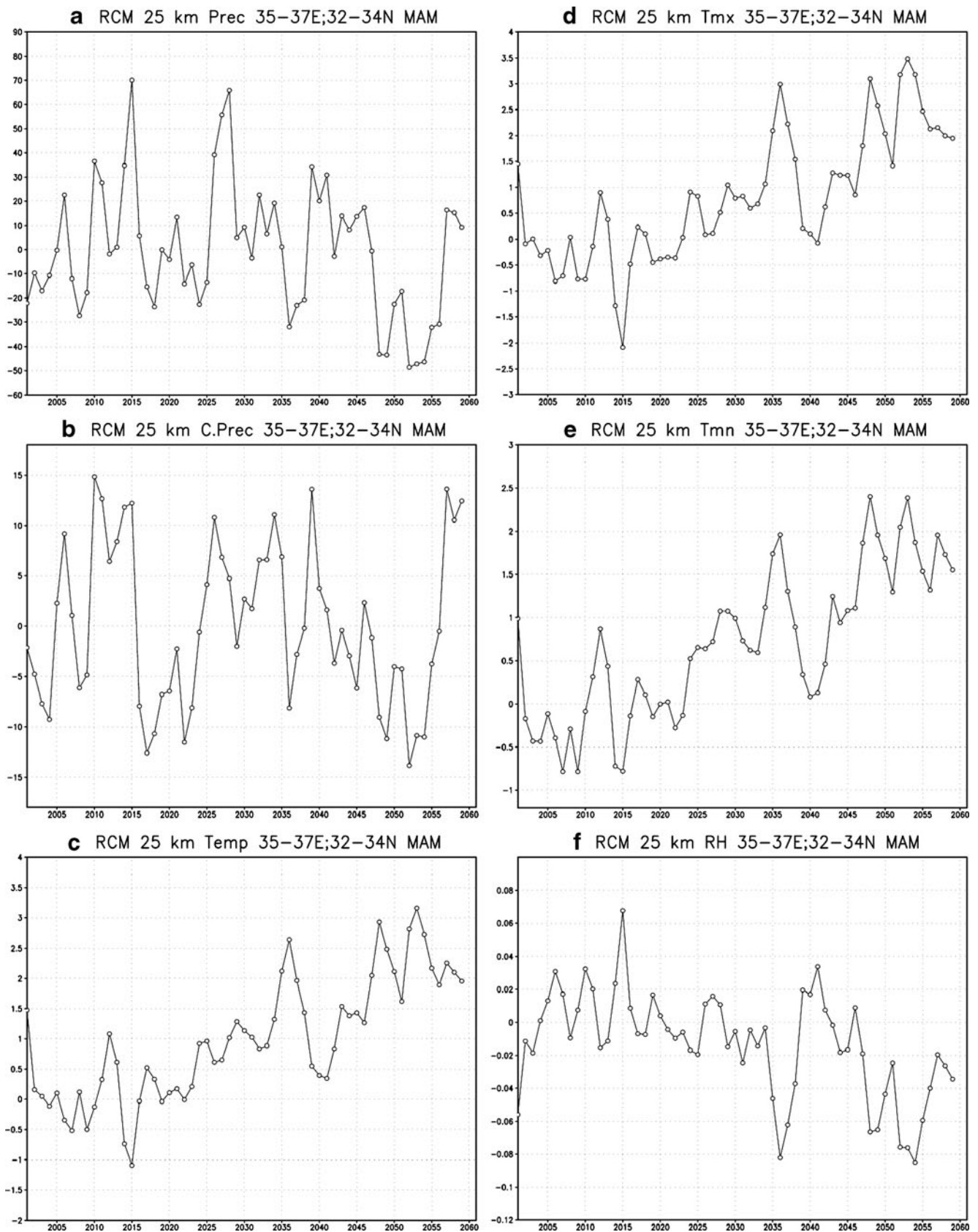


Fig. 13 Same as in Figs. 12 but for MAM

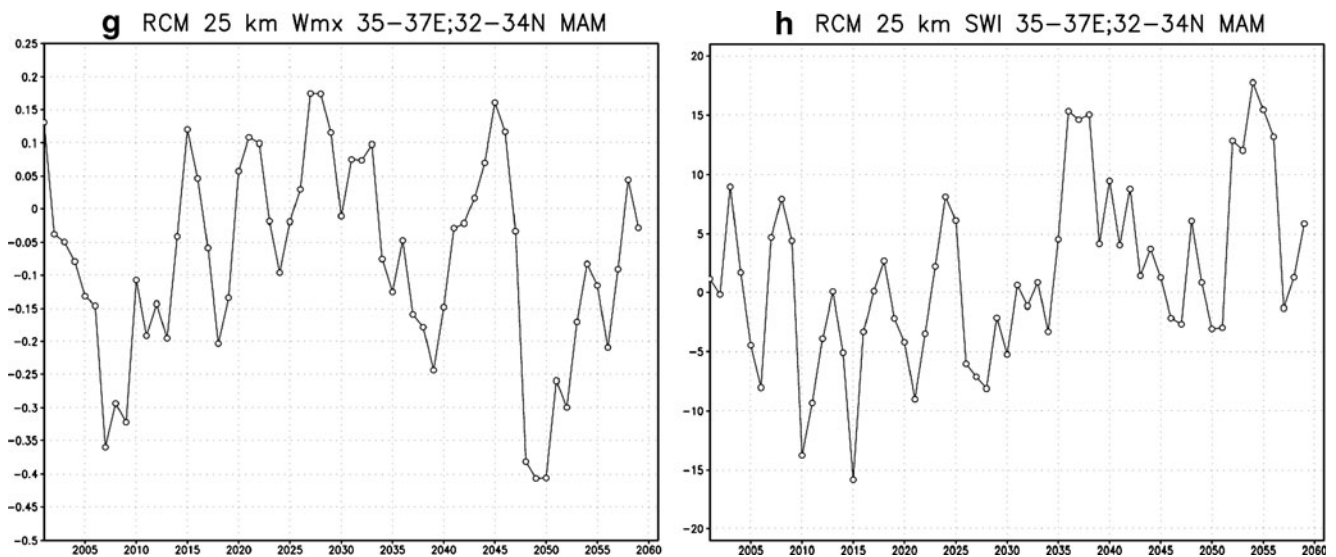


Fig. 13 (continued)

trend is significantly more notable over the Middle East ($>0.6^{\circ}\text{C decade}^{-1}$) and Asia Minor ($0.5^{\circ}\text{C decade}^{-1}$). The air temperature rise during autumn (SON) varies from $\sim 0.2^{\circ}\text{C decade}^{-1}$ over the ECM to $0.3^{\circ}\text{C decade}^{-1}$. It is of interest to note that the patterns in Fig. 8a-d and Fig. 9a-d well agree qualitatively with similar patterns obtained by simple subtraction of multi-year mean seasonal precipitation and air temperature simulated in the experiment for years 2031-2060 and 1961-1990 (imitation of time slice strategy, not presented). The “time-slice” and “transient” trend patterns for precipitation differ significantly over the EM and ECM. In particular, the “time-slice” approach does not capture the intense (and significant) precipitation drop over the near-coastal Mediterranean zone found in the patterns for DJF and SON (Fig. 8a, d). At the same time, no significant differences between the “transient” and “time-slice” patterns for air-temperature have been detected. The fact appears to be demonstrating that increases in the period of time averaging result in a notable decrease in the influence of the physically based variability on the climate change signal. The effect is more significant in the simulated variations in precipitation than in those for the air temperatures, which appear more dependent on effects of the larger scales.

5 Time variations in the climate change trend over ECM

5.1 Role of small-scale effects

To estimate the role of small-scale effects in the climate change trend projected, time series of the differences

between the 50 and 25 km ECM area-averaged seasonal (separately for each of the seasons) precipitation and near surface air-temperatures are given in Fig. 10a-d and Fig. 11a-d. The two (50 and 25 km) runs project quite similar (although differing by amplitudes) trends of other parameters as well (not presented). As follows from Fig. 10a, the graph with precipitation difference varies from 2.5 to -2.5 mm day^{-1} during winter (DJF). Amplitude of the oscillations is somewhat smaller in the figures for autumn (Fig. 10d) and spring (Fig. 10b). The differences for summer are significantly smaller (-0.1 to 0.1 mm day^{-1} ; Fig. 10c). The amplitude of the oscillations in difference between amounts of summer precipitation (JJA) produced in the 50 and 25 km runs during the later years 2050-2060 suggest the inability of the coarser resolution 50 km run to represent small-scale processes. For the simulated DJF and MAM T2m, differences are gradually increasing from 0.2°C to 0.8°C and from 0.1°C to 0.7°C , respectively. This is perhaps a consequence of excessive warming in the 50 km run due to underproduction of precipitation and clouds. Results from the double resolution experiment suggest an increase in the role of convective precipitation under the warmer climate conditions during years 2001-2060, as can be seen in the increase in precipitation in the 25 km model which better captures these local convective processes. The situation is somewhat different in the cases of summer [and autumn] seasons (Fig. 11c-d). Namely, during the seasons the simulated 50 minus 25 km air temperature differences are negative. Absolute values of the differences increase with time from $\sim 0^{\circ}\text{C}$ - 0.4°C [-0.25°C to -0.8°C] during 2001-2060 (i.e., the 50 km experiment systematically produces lower T2m values, indicating overproduction of precipitation in the 50 km run).

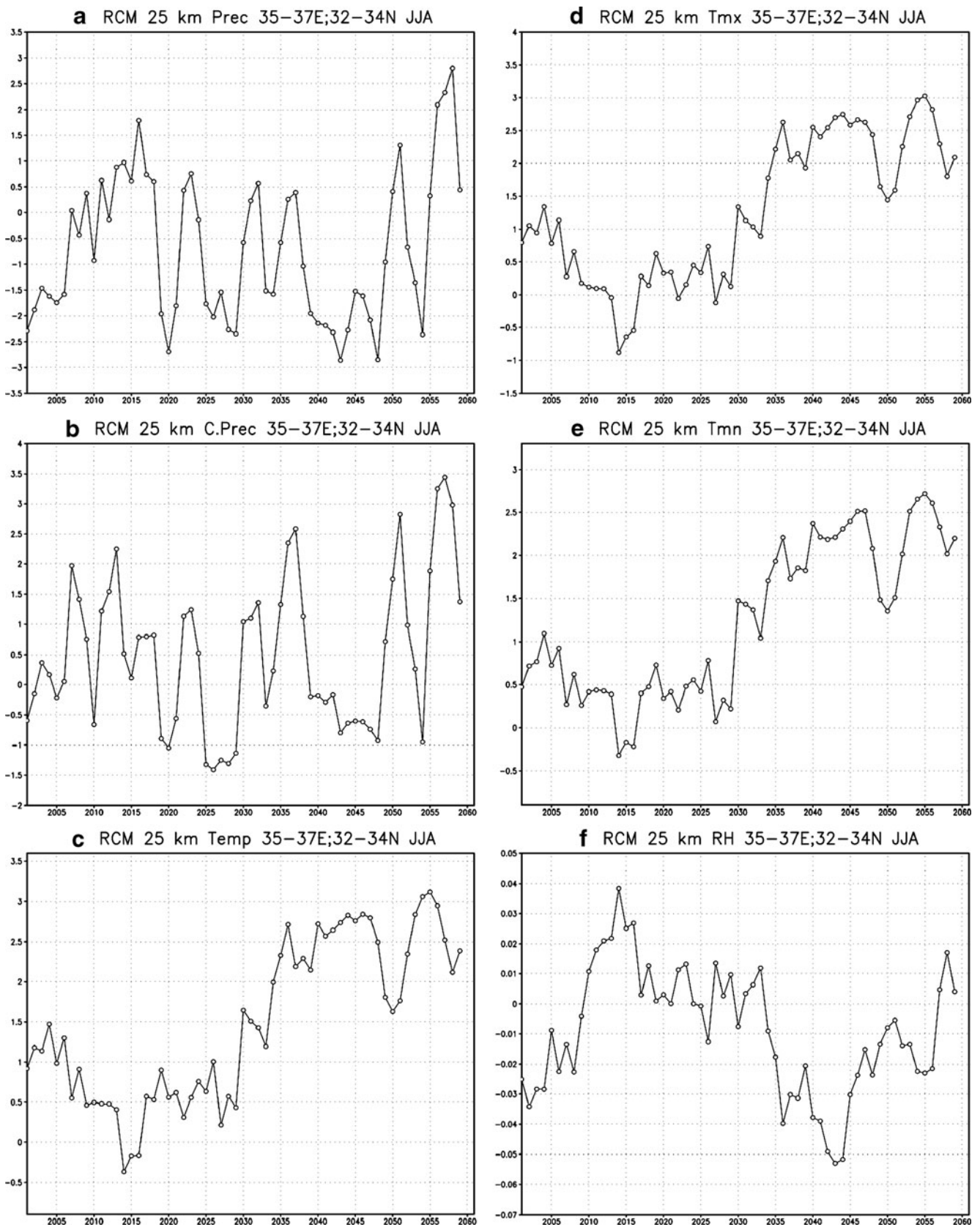


Fig. 14 Same as in Figs. 12 but for JJA

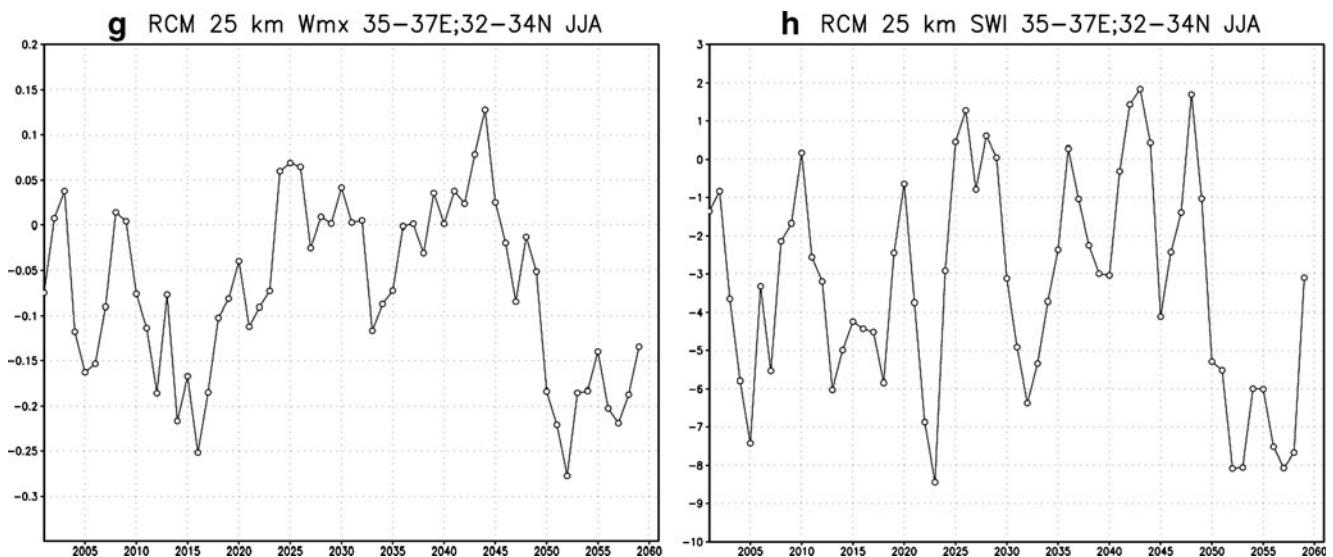


Fig. 14 (continued)

5.2 Projections of regional climate trend

Results of the experiment focusing on the inter-decadal time variability of the projected 2001–2060 climate change trends over the ECM have been evaluated based on an approach similar to that suggested by Giorgi (2005). The quantities being discussed are the “climate changes”, i.e., the differences between the model simulated area average values of different climate parameters at each year and those representing “present day” conditions (reference 1961–1990 averages). In contrast with Giorgi (2005) no strong time filtering of the original time-series was applied however. Only a 3-year running average of the original time series was performed in order to reduce the effects of the interannual variability in the model data without affecting the inter-decadal one.

Model simulated area-averaged ECM time series of the following quantities (a) total precipitation, (b) convective precipitation, (c) anemometer (2 m) temperature, (d) maximum anemometer temperature, (e) minimum anemometer temperature, (f) relative humidity, (g) maximum wind magnitude and (h) short-wave incident radiation are discussed here. The time series are presented in Fig. 12a–h; Fig. 15a–h separately for DJF, MAM, JJA, and SON.

In general, the results can be divided into two separate periods: (a) 2001–2020 and (b) 2021–2060. These periods exhibit opposite trends in a number of the parameters evaluated. This trend is also seen in the driving ECHAM5 data (not presented). During winter (DJF) (Fig. 12a–h), the RCM experiment projects increases in mean seasonal total precipitation amount ($20.5 \text{ mm month}^{-1}$) from 2001 till 2015–2020 and a consequent gradual 60 mm month^{-1} drop in precipitation

(Fig. 12a). A minor gradual decline in amount of DJF convective precipitation is also projected (Fig. 12b). Simulated climate change processes during 2001–2060 are characterized by a gradual rise in anemometer air temperature as well as the temperature extremes (minimum and maximum temperatures (Fig. 12c–e). The simulated ECM climate change process is characterized by an insignificant rise in relative humidity until ~ 2020 followed by a gradual drop in the parameter during 2020–2060 (Fig. 12f), as well as a decline in the amount of solar incident radiation until ~ 2020 followed by its rise during the rest of the period (Fig. 12h). The trends are consistent with those in the total precipitation projected. Projected rise in maximum wind speed of $\sim 0.8 \text{ ms}^{-1}$ (Fig. 12g) from 2001 till 2020 followed by a 1 ms^{-1} drop during 2020–2060 are also consistent with the trends in total precipitation shown in Fig. 12a.

During spring (Fig. 13a–h) the experiment projects an increase in total precipitation amount of $\sim 80 \text{ mm month}^{-1}$ until ~ 2015 , followed by a gradual 90 mm month^{-1} drop in precipitation amount during 2020–2060 (Fig. 13a). Also the rate of monthly mean area average convective precipitation in the ECM increases to $\sim 50 \text{ mm month}^{-1}$ during the 2001–2015 time period and then declines by $\sim 40 \text{ mm month}^{-1}$ during the rest of the period (Fig. 13b). As in the DJF case, the experiment projects a gradual rise in the MAM air temperature, as well as minimum and maximum air temperature ($\sim 3.0^\circ\text{C}$) during 2001–2060 (Fig. 13b–d). As above the projected MAM trends in relative humidity and incident solar radiation appear to be resulting from those in total precipitation (Fig. 13a). Relative humidity is projected to rise from 2001 to 2010 and then to drop quite slowly (Fig. 13f). The time-period

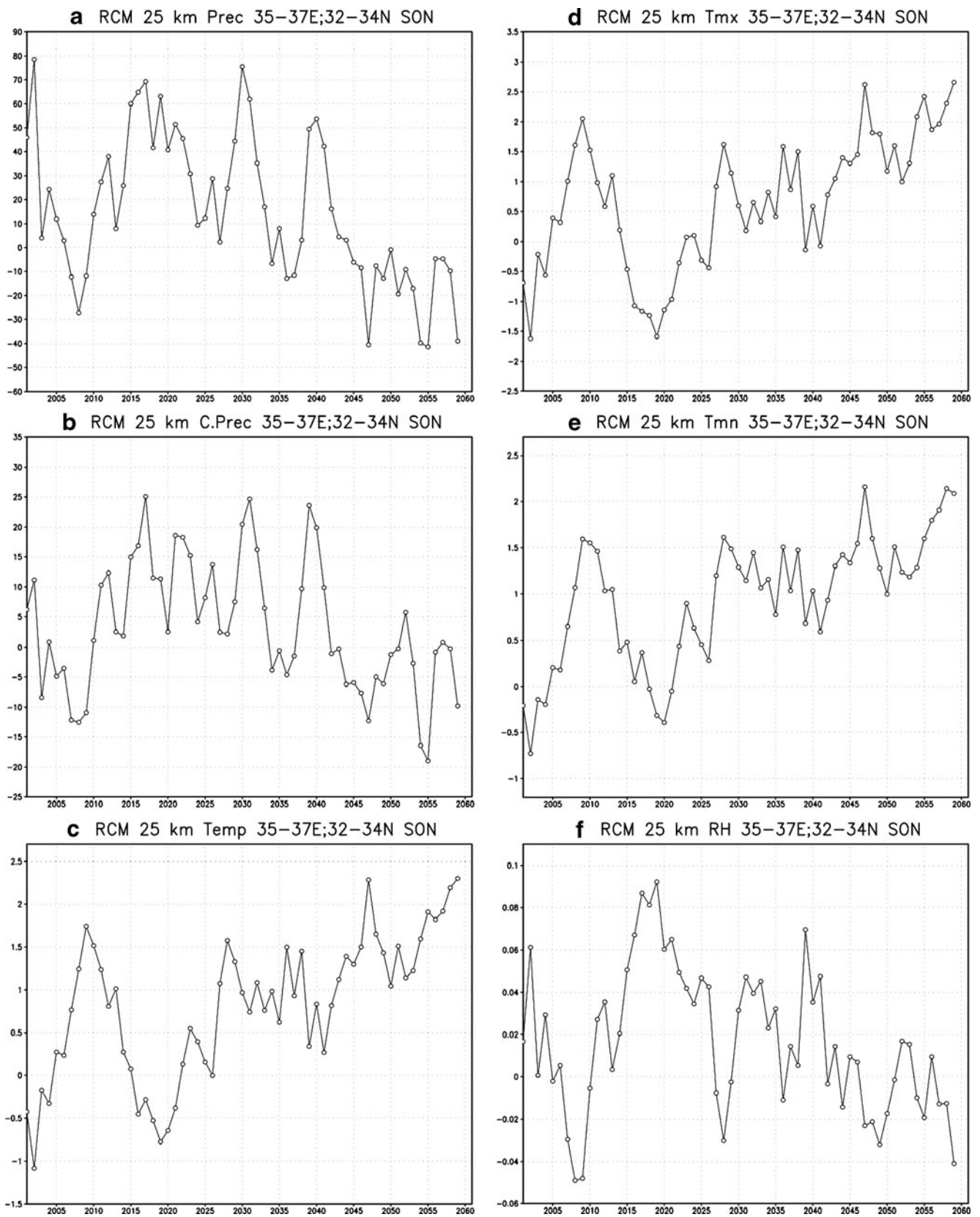


Fig. 15 Same as in Figs. 12 but for SON

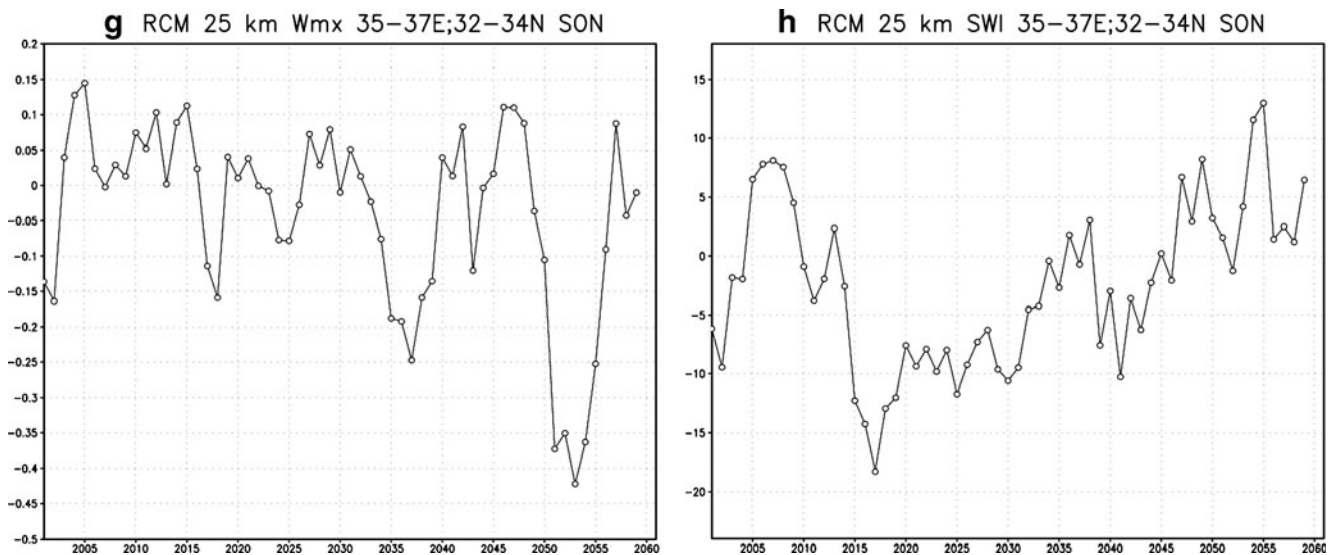


Fig. 15 (continued)

till 2060 in the simulation results is characterized by a drop in amount of incident solar radiation till ~2015 followed by its minor rise (Fig. 13h; $\sim 20 \text{ Wt m}^{-2}$).

The experiment projects a gradual drop in total summer precipitation during 2001–2050 followed by rise in later years (Fig. 14a). The rate of mean monthly convective precipitation is increasing however in the experiment's projection (Fig. 14b). Simulated monthly mean, as well as the minimum and maximum near surface air temperatures (Fig. 14c–e) during summer are rising from 2001 to 2030–2040 and then remain quasi-constant. Relative humidity (Fig. 14f) in the RCM results is rising from 2001 to ~2015. The experiment projects minimal changes in near surface relative humidity during summer, a minor rise in maximum wind velocity until 2015 (Fig. 14g) and a rise in the amount of incident solar radiation until 2050 (Fig. 14h).

During autumn the experiment projects a rise in total precipitation amount until 2015–2020 with consequent drop in later years (Fig. 15a). Similar behavior is also projected for convective precipitation (Fig. 15b). In an accord with the trend the experiment also projects air temperature (mean, maximum, minimum) decrease until ~2020 and a rise thereafter (Fig. 15c–e). Also in accord with the trend in total precipitation simulated area-averaged seasonal values of relative humidity (Fig. 15f; solar incident radiation (Fig. 15h)) are rising (declining) from 2001 to 2020 and declining (rising) afterwards. The values of monthly mean maximum wind speed projected for autumn (Fig. 15g) are not affected by the global warming trends, however.

6 Overview and discussion

This study's overall aim was to estimate dynamically based future regional climate change trend projections over the EM, focusing on the Israeli sub-region. A double resolution regional climate change simulation experiment over the eastern Mediterranean region for the period from 1960 to 2060 has been performed.

The RCM experiment qualitatively confirms earlier projections (Giorgi et al. 2004b; Krichak et al. 2007, 2009a) on notable climate changes in the ECM region during the first half of 21st century. Application of the double-resolution transient climate simulation strategy allowed a more detailed analysis of the process. A statistically significant positive trend in near-surface air temperature during the four seasons of year characterizes results of the experiment over the whole EM region during 2001–2060. The experimental projection of climate change also includes a notable, significant negative precipitation trend during DJF and SON over the ECM. The experiment also consistently projects a minor positive precipitation trend during MAM and negative precipitation trend during JJA. The trends are not significant over the area, however. The result is a consequence of relatively low frequency of rainy events during MAM and practically absolute absence of rains during JJA. Obtaining more statistically significant trend estimates for the seasons would require more data (i.e., using daily RCM data or performing simulations for longer time periods). Also projected are the rises in the air temperature extremes as well as in relative contribution of convective processes in the ECM region during 2020–2060

as a result of projected decline in amount of total precipitation but a zero trend in that of convective one. Comparison of results of the simulations with 50 km/14 L and 25 km/18 L reveals a notable sensitivity of the projected larger-scale climate change signals to smaller-scale effects. Projected multi-decadal variations of air-temperature and its extremes, maximum wind speed and solar incident radiation flux over the ECM are clearly controlled by those in total precipitation.

Acknowledgments The helpful comments by reviewers are acknowledged with gratitude. The research was supported by the German-Israeli research grant (GLOWA, Jordan River) through the Israeli Ministry of Science and Technology and the German Bundesministerium fuer Bildung und Forschung (BMBF), a research grant from the Water Authority of Israel, as well as by the European Commission's Sixth Framework Programme, Priority 1.1.6.3 Global Change and Ecosystems (CIRCE), Contract no.:036961. P. Kunin actively participated in planning and realization of a first stage of the experiment. We are grateful to Filippo Giorgi, Xunqiang Bi and Sara Rauscher of the Physics of Weather and Climate (PWC) Section of the Abdus Salam International Centre for Theoretical Physics (ICTP), Trieste for providing expertise on using RegCM3 as well as the driving data from ECHAM5 climate change simulation experiment at the MPI-M, Hamburg. A Matlab code by Simone Fatichi has been used for performing Mann-Kendall significance test.

References

- Caya D, Biner S (2004) Internal variability of RCM simulations over an annual cycle. *Climate Dynamics* 22:33–46
- Christensen JH, Christensen OB (2003) Climate modelling: severe summertime flooding in Europe. *Nature* 421:805–806
- Evans JP, Smith RB, Oglesby RJ (2004) Middle East climate simulation and dominant precipitation processes. *Int J Climatol* 24:1671–1694
- Giorgi F (2005) Interdecadal variability of regional climate change: implications for the development of regional climate change scenarios. *Meteorol Atmos Phys* 89:1–15. doi:10.1007/s00703-005-0118-y
- Giorgi F, Bi X, Pal JS (2004a) Mean, interannual variability and trends in a regional climate change experiment over Europe. I. Present-day climate (1961–1990). *Clim Dyn* 22:733–756
- Giorgi F, Bi X, Pal JS (2004b) Mean, interannual variability and trends in a regional climate change experiment over Europe. II. climate change scenarios (2071–2100). *Clim Dyn* 23:839–858
- Gubasch U (2001) Simulations of regional climate change. In: Lozan JL, Grassl H, Hupfer P (eds) *Climate of 21st century: changes and risks*. Scientific facts. ISBN 3-00-006227-0, 448pp
- Hagemann S, Göttel H, Jacob D, Lorenz P, Roeckner E (2008) Projected changes of the hydrological cycle over large European catchments as simulated by the MPI-M global and regional climate models. *Geophysical Research Abstracts*, 10, EGU2008-A-01136, SRef-ID: 1607-7962/gra/EGU2008-A-01136
- Heckl A, Kunstmann H (2009) High resolution transient regional climate simulations for the Eastern Mediterranean. *Geophysical Research Abstracts*, 11, EGU2009-10230
- IPCC (2001) *Climate change 2001: the scientific basis, contribution of Working Group I to the Third Assessment Report of the Intergovernmental Panel on Climate Change*. In: Houghton JT et al (eds). Cambridge University Press, Cambridge, UK, pp 881
- IPCC (2007) *Climate change - the physical science basis*. In: Solomon S, Qin D, Manning M, Chen Z, Marquis M, Averyt KB, Tignor M, Miller HL (eds) *Contribution of working group I to the fourth assessment report of the intergovernmental panel on climate change*. Cambridge University Press, Cambridge, p 996
- Jones RG, Murphy JM, Noguer M (1995) Simulation of climate change over Europe using a nested regional climate model I: assessment of control climate, including sensitivity to location of lateral boundary conditions. *Q J R Meteorol Soc* 121:1413–1449
- Jones RG, Murphy JM, Noguer M, Keen M (1997) Simulation of climate change over Europe using a nested regional climate model II: comparison of driving and regional model responses to a doubling of carbon dioxide. *Q J R Meteorol Soc* 123:265–292
- Kendall MG, Dickinson Gribbons J (1990) *Rank correlation methods* (Charles Griffin Book Series), 5th edn, 272 p
- Köppen W, Geiger R (1936) *Das geographische system der klimate*. In: Köppen W, Geiger R (eds) *Handbuch der klimatologie*. Bd 1, Teil C, Verlag Gebrüder Bornträger, Berlin, p 44
- Krichak SO (2008) Regional climate model simulation of present-day regional climate over the European part of Russia with RegCM3. *Russian Meteorology and Hydrology*, 2008, Vol. 33, No. 1, pp. 20–26. _ Allerton Press, Inc., (Original Russian Text _ S.O. Krichak, 2008, published in *Meteorologiya i Gidrologiya*, 2008, No. 1, pp. 31–41)
- Krichak SO, Alpert P (2010) Projection of climate change during first half of twenty-first century over the Eastern Mediterranean region according to results of a transient RCM experiment with 25 km resolution. *Geophysical Research Abstracts*, 12, EGU2010
- Krichak SO, Alpert P, Krishnamurti TN (1997) Interaction of topography and tropospheric flow—a possible generator for the red sea trough? *Meteorol Atmos Phys* 63(3-4):149–158
- Krichak SO, Alpert P, Dayan M (2004) The role of atmospheric processes associated with hurricane Olga in the December 2001. *J Hydrometeorology* 5(6):1259–1270
- Krichak SO, Alpert P, Bassat K, Kunin P (2007) The surface climatology of the eastern Mediterranean region obtained in a three-member ensemble climate change simulation experiment. *Advances in Geosciences Adv Geosci* 12:67–80. www.adv-geosci.net/12/67/2007
- Krichak SO, Alpert P, Kunin P (2009a) Projections of climate change over non-boreal east Europe during first half of twenty-first century according to results of a transient RCM experiment. In: Groisman PYa, Ivanov SV (eds) *Regional aspects of climate-terrestrial-hydrologic interactions in non-boreal eastern Europe*. Springer, NATO Science for Peace and Security Series, Series C: Environmental Security, pp 55–62
- Krichak SO, Alpert P, Kunin P (2009b) Numerical simulation of seasonal distribution of precipitation over the Eastern Mediterranean with a RCM. *Climate Dynamics*. doi:10.1007/s00382-009-0649-x
- Leckebusch CC, Ulbrich U (2004) On the relationship between cyclones and extreme windstorm events over Europe under climate change. *Global Planet Change* 44:181–193
- Mann HB (1945) Nonparametric tests against trend. *Econometrica* 13:245–259
- Meehl GA, Washington WM, Arblaster JM, Bettge TW, Strand WG (2000) Anthropogenic forcing and decadal climate variability in sensitivity experiments of twentieth- and twenty-first century climate. *J Clim* 13(21):3728–3744
- Mitchell TD, Carter TR, Jones PD, Hulme M, New M (2004) A comprehensive set of high-resolution grids of monthly climate for Europe and the globe: the observed record (1901–2000) and 16 scenarios (2001–2100). Tyndall Centre Working Paper No. 55, Tyndall Centre for Climate Change Research. University of East Anglia, Norwich

- Muller WA, Roeckner E (2008) ENSO teleconnections in projections of future climate in ECHAM5/MPI-OM. *Clim Dyn*. doi:10.1007/s00382-007-0357-3
- Onol B (2008) Examining future climatic impact over Eastern Mediterranean using a regional climate model ESF-MedCLIVAR Workshop on Climate Change Modelling for the Mediterranean Region. Trieste, Italy
- Pal JS, Giorgi F, Bi X, Elguindi N, Solmon F, Gao X, Rauscher SA, Francisco R, Zakey A, Winter J, Ashfaq M, Syed FS, Bell JL, Diffenbaugh NS, Karmacharya J, Konaré A, Martinez D, da Rocha RP, Sloan LC, Steiner AL (2007) Regional climate modeling for the developing world: The ICTP RegCM3 and RegCNET. *Bull Amer Meteor Soc* 88:1395–1409
- Raupach MR, Marland G, Ciais PH, Le Quéré C, Canadell JG, Klepper G, Field CB (2007) Global and regional drivers of accelerating CO₂ emissions. *Proc of the Nat Acad Sci USA*. doi:10.1073/pnas.0700609104
- Rial JA, Pielke RA Sr, Beniston M, Claussen M, Canadell J, Cox P, Held H, De Noblet-Ducoudre N, Prinn R, Reynolds JF, Salas JD (2004) Nonlinearities, feedbacks, and critical thresholds within the Earth's climate system. *Clim Change* 65: 11–38
- Rodwell MJ, Hoskins B (1996) Monsoons and the dynamic of deserts. *Q J Roy Meteorol Soc* 122:1385–1404
- Samuels R, Rimmer A, Krichak SO, Alpert P (2009) Climate change impacts on the Jordan River, Israel: downscaling application from a regional climate model. *J Hydrometeorology* (in press)
- Takle ES, Roads J, Rockel B, Gutowski WJ, Arritt R, Menke I, Jones CG, Zadra A (2007) Transferability intercomparison: an opportunity for new insight on the global water cycle and energy budget. *Bull Amer Meteorol Soc* 88:375–384
- Ulbrich U, Christoph M (1999) A shift of the NAO and increasing storm track activity over Europe due to anthropogenic greenhouse gas forcing. *Climate Dynamics* 15:551–559
- Wang Y, Leung LR, McGregor JL, Lee DK, Wang W-C, Ding Y, Kimura F (2004) Regional climate modeling: progress, challenges, and prospects. *J Meteorol Soc Japan* 82(6):1599–1628
- Ziv B, Dayan U, Sharon D (2005) A mid-winter, tropical extreme flood-producing storm in southern Israel: synoptic scale analysis. *Meteorol Atmos Phys* 88(1–2):53–63
- Ziv B, Saaroni H, Romem M, Heifetz E, Harnik N, Baharad A (2010) Analysis of conveyor belts in winter Mediterranean cyclones. *Theor Appl Climatol* 99:441–455. doi:10.1007/s00704-009-0150-9